Supplement of Geosci. Model Dev., 18, 1785–1808, 2025
https://doi.org/10.5194/gmd-18-1785-2025-supplement

Geoscientific Model Development
Open Access

Supplement of

A rapid-application emissions-to-impacts tool for scenario assessment: Probabilistic Regional Impacts from Model patterns and Emissions (PRIME)

Camilla Mathison et al.

Correspondence to: Camilla Mathison (camilla.mathison@metoffice.gov.uk)

1 Ensemble selection from temperature and CO_2 distribution

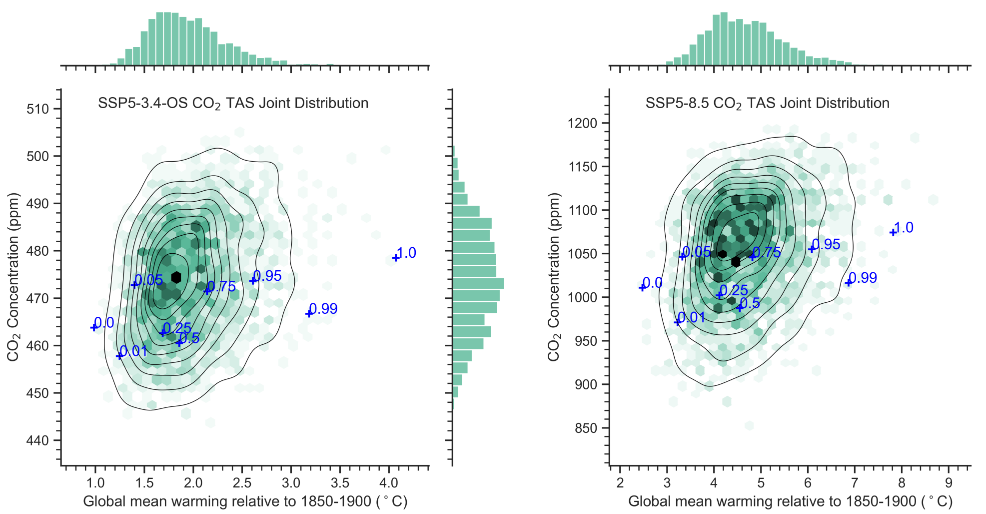

Figure S1. Joint frequency distribution from the FaIR simulations of Temperature (TAS) and CO_2 concentration in 2100 for SSP5-3.4-OS (left) and the scenario used to train PRIME: SSP5-8.5 (right) and the sub-selected percentiles (blue crosses) used to drive the JULES impacts model. Shades of green denote the density of points with individual histograms shown above and to the right of the main panel. 10% confidence intervals are shown by the contours.

2 Evaluation of the patterns

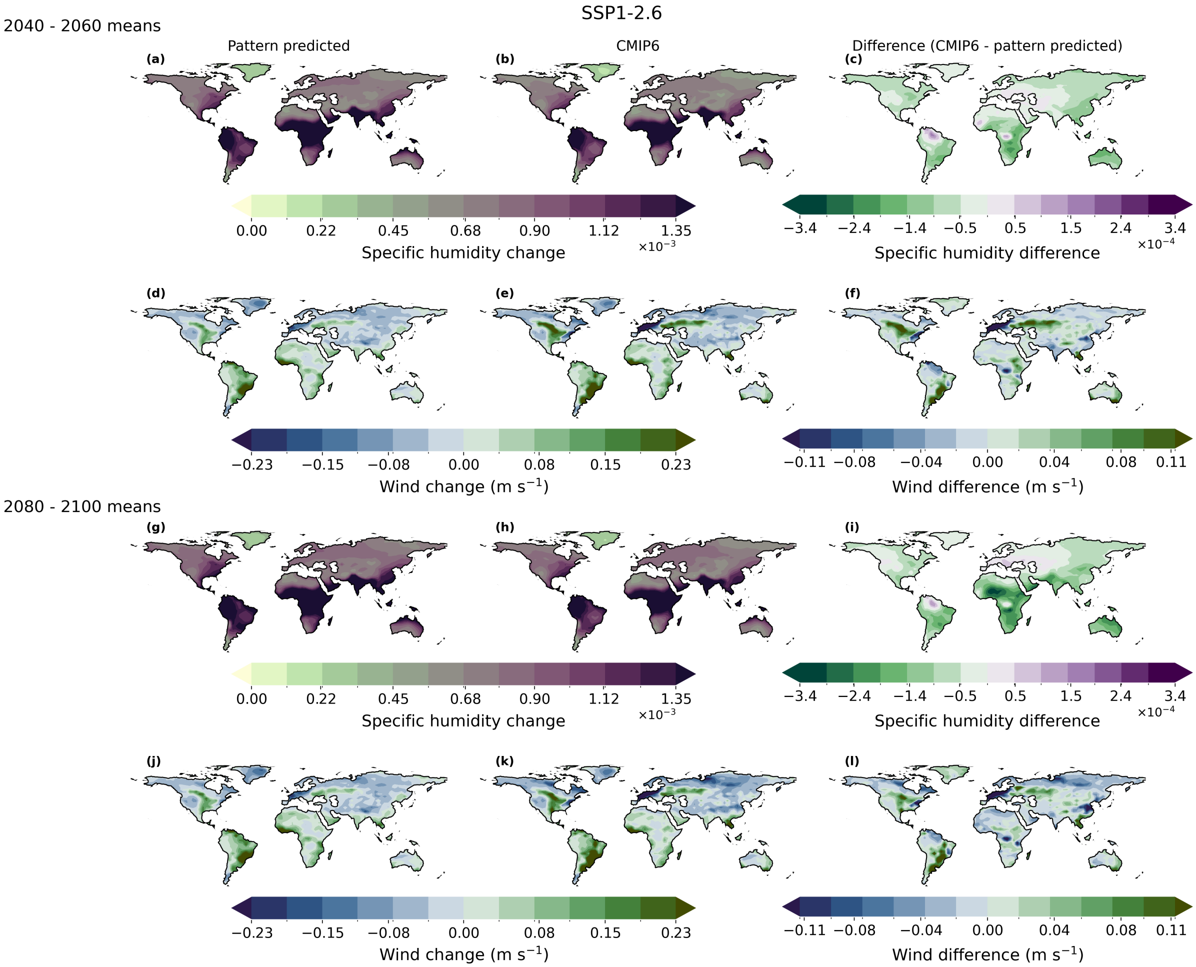

Figure S2. Evaluation of the pattern predicted ensemble mean anomalies compared to the CMIP6 ensemble mean anomalies for near-surface specific humidity **(a-c, g-i)** and wind **(d-f, j-l)** for SSP1-2.6. Maps **(a-f)** highlight mid-century predictions, and **(g-l)** show those for the end of century. The right hand column shows the difference between the predictions (left hand column) and CMIP6 (middle column).The colourbar for the differences is not the same as that for the anomalies, in order to show the detail in the prediction error, which is small compared to the change induced by the scenario.

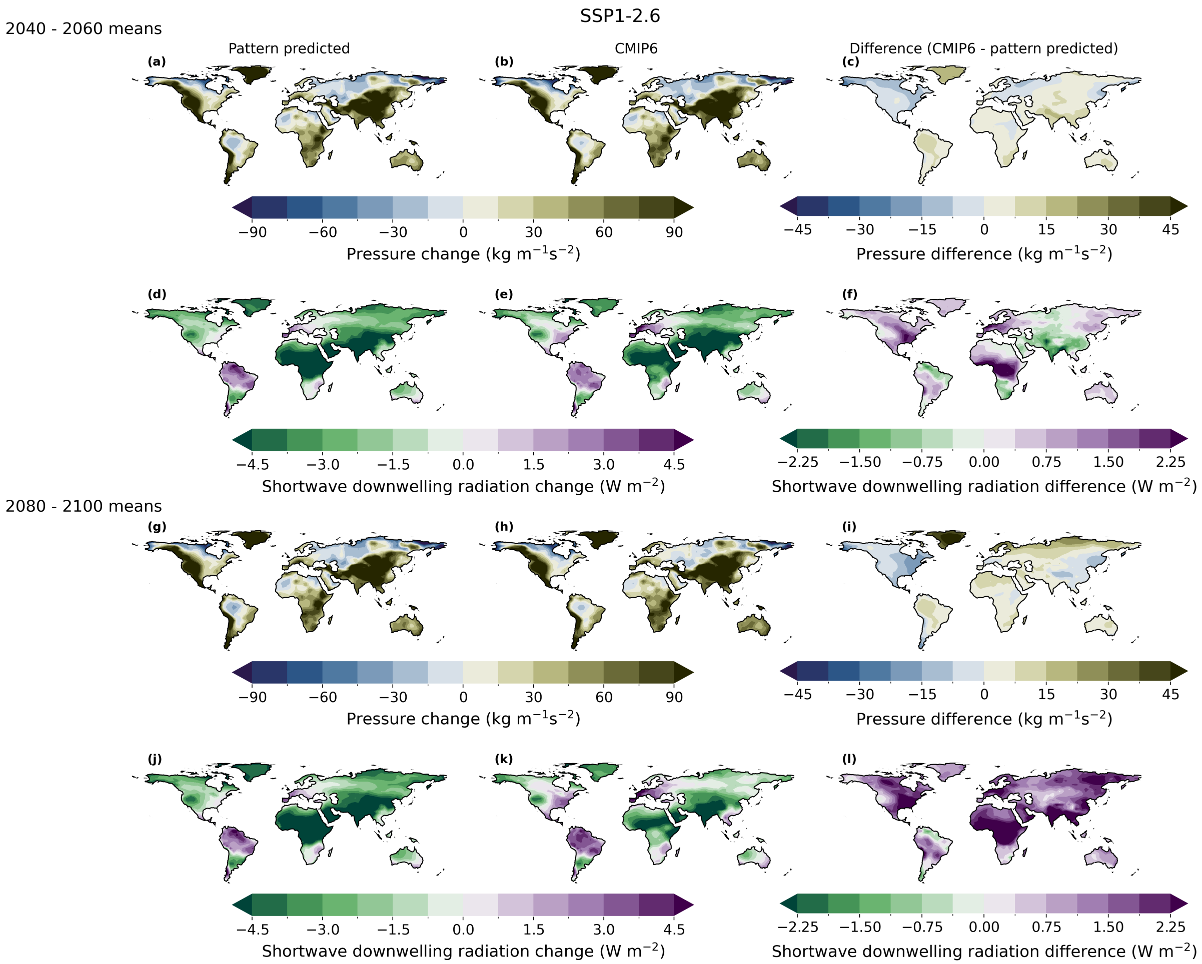

Figure S3. Evaluation of the pattern predicted ensemble mean anomalies compared to the CMIP6 ensemble mean anomalies for near-surface pressure **(a-c, g-i)** and shortwave downwelling radiation **(d-f, j-l)** for SSP1-2.6. Maps **(a-f)** highlight mid-century predictions, and **(g-l)** show those for the end of century. The right hand column shows the difference between the predictions (left hand column) and CMIP6 (middle column).The colourbar for the differences is not the same as that for the anomalies, in order to show the detail in the prediction error, which is small compared to the change induced by the scenario.

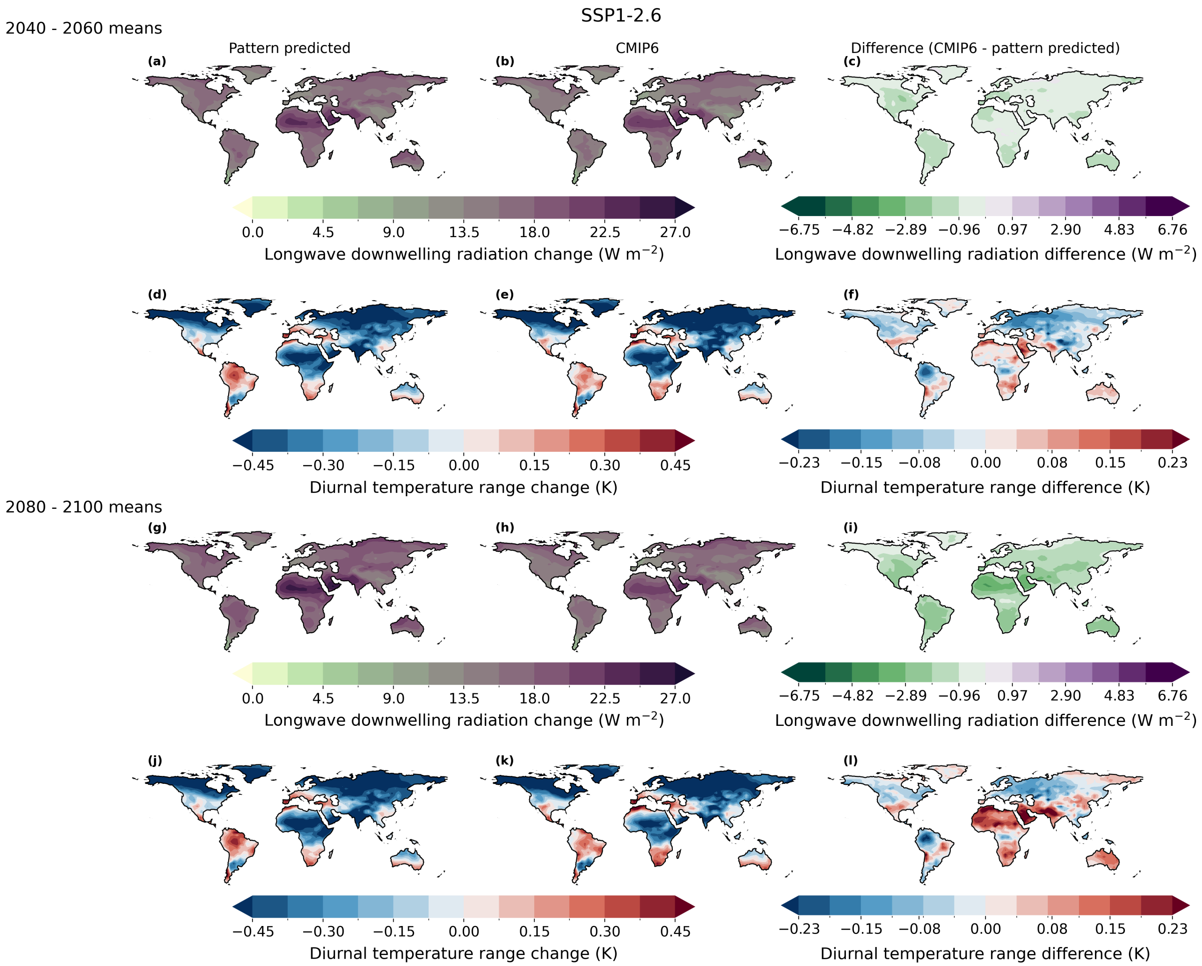

Figure S4. Evaluation of the pattern predicted ensemble mean anomalies compared to the CMIP6 ensemble mean anomalies for longwave downwelling radiation **(a-c, g-i)** and diurnal temperature range **(d-f, j-l)** for SSP1-2.6. Maps **(a-f)** highlight mid-century predictions, and **(g-l)** show those for the end of century. The right hand column shows the difference between the predictions (left hand column) and CMIP6 (middle column).The colourbar for the differences is not the same as that for the anomalies, in order to show the detail in the prediction error, which is small compared to the change induced by the scenario.

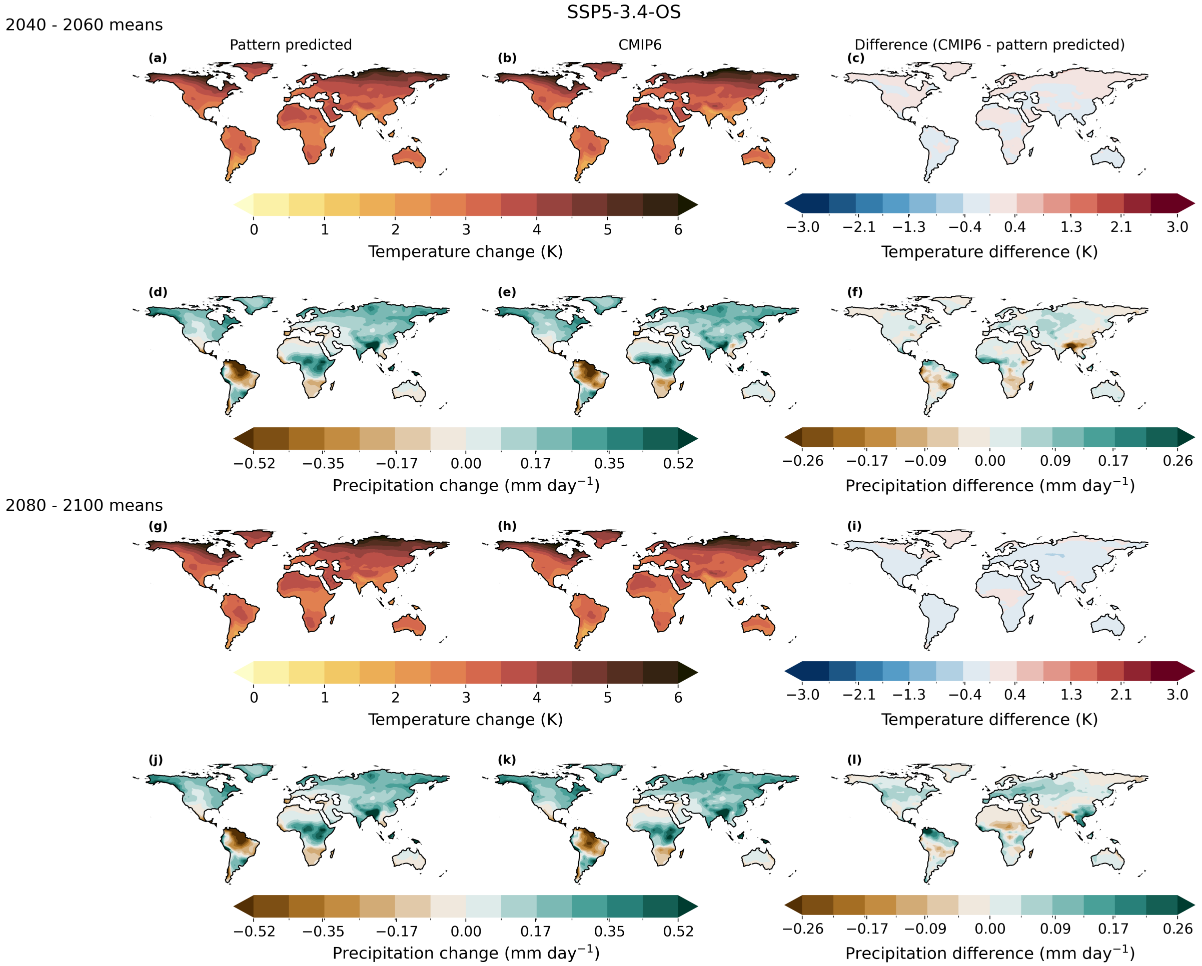

Figure S5. Evaluation of the pattern predicted ensemble mean anomalies compared to the CMIP6 ensemble mean anomalies for temperature **(a-c, g-i)** and precipitation **(d-f, j-l)** for SSP5-3.4-OS. Maps **(a-f)** highlight mid-century predictions, and **(g-l)** show those for the end of century. The right hand column shows the difference between the predictions (left hand column) and CMIP6 (middle column).The colourbar for the differences is not the same as that for the anomalies, in order to show the detail in the prediction error, which is small compared to the change induced by the scenario.

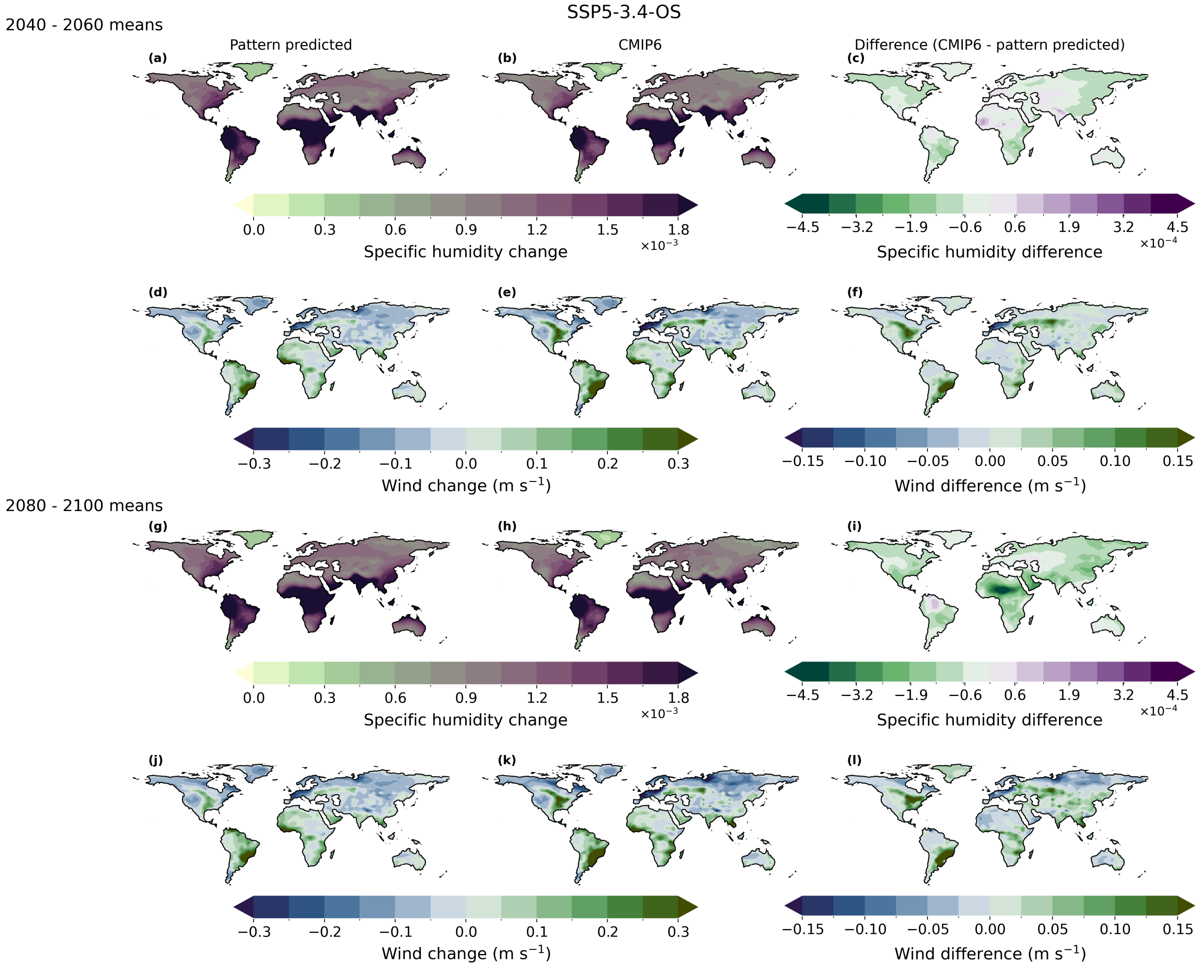

Figure S6. Evaluation of the pattern predicted ensemble mean anomalies compared to the CMIP6 ensemble mean anomalies for near-surface specific humidity **(a-c, g-i)** and wind **(d-f, j-l)** for SSP5-3.4-OS. Maps **(a-f)** highlight mid-century predictions, and **(g-l)** show those for the end of century. The right hand column shows the difference between the predictions (left hand column) and CMIP6 (middle column). The colourbar for the differences is not the same as that for the anomalies, in order to show the detail in the prediction error, which is small compared to the change induced by the scenario.

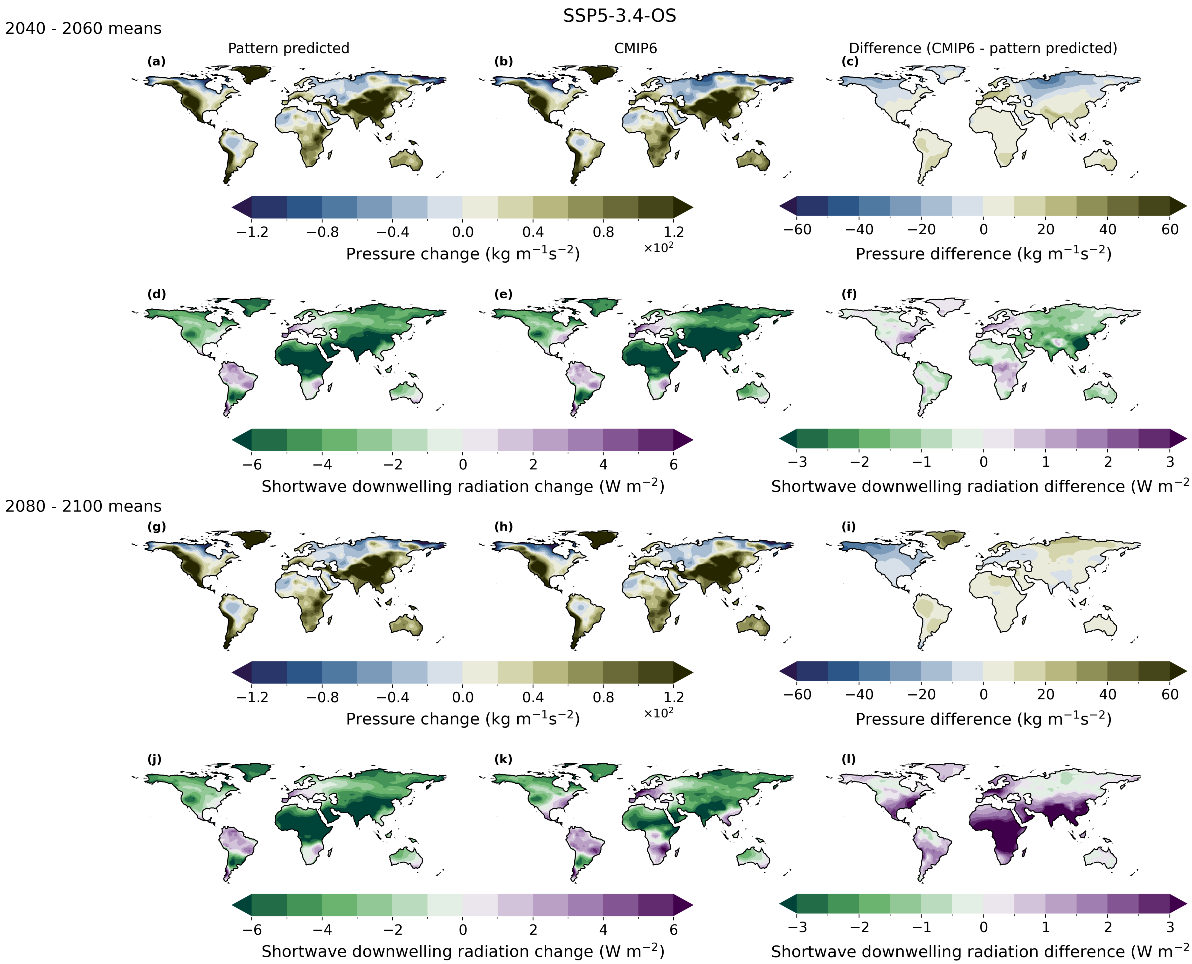

Figure S7. Evaluation of the pattern predicted ensemble mean anomalies compared to the CMIP6 ensemble mean anomalies for near-surface pressure **(a-c, g-i)** and shortwave downwelling radiation **(d-f, j-l)** for SSP5-3.4-OS. Maps **(a-f)** highlight mid-century predictions, and **(g-l)** show those for the end of century. The right hand column shows the difference between the predictions (left hand column) and CMIP6 (middle column). The colourbar for the differences is not the same as that for the anomalies, in order to show the detail in the prediction error, which is small compared to the change induced by the scenario.

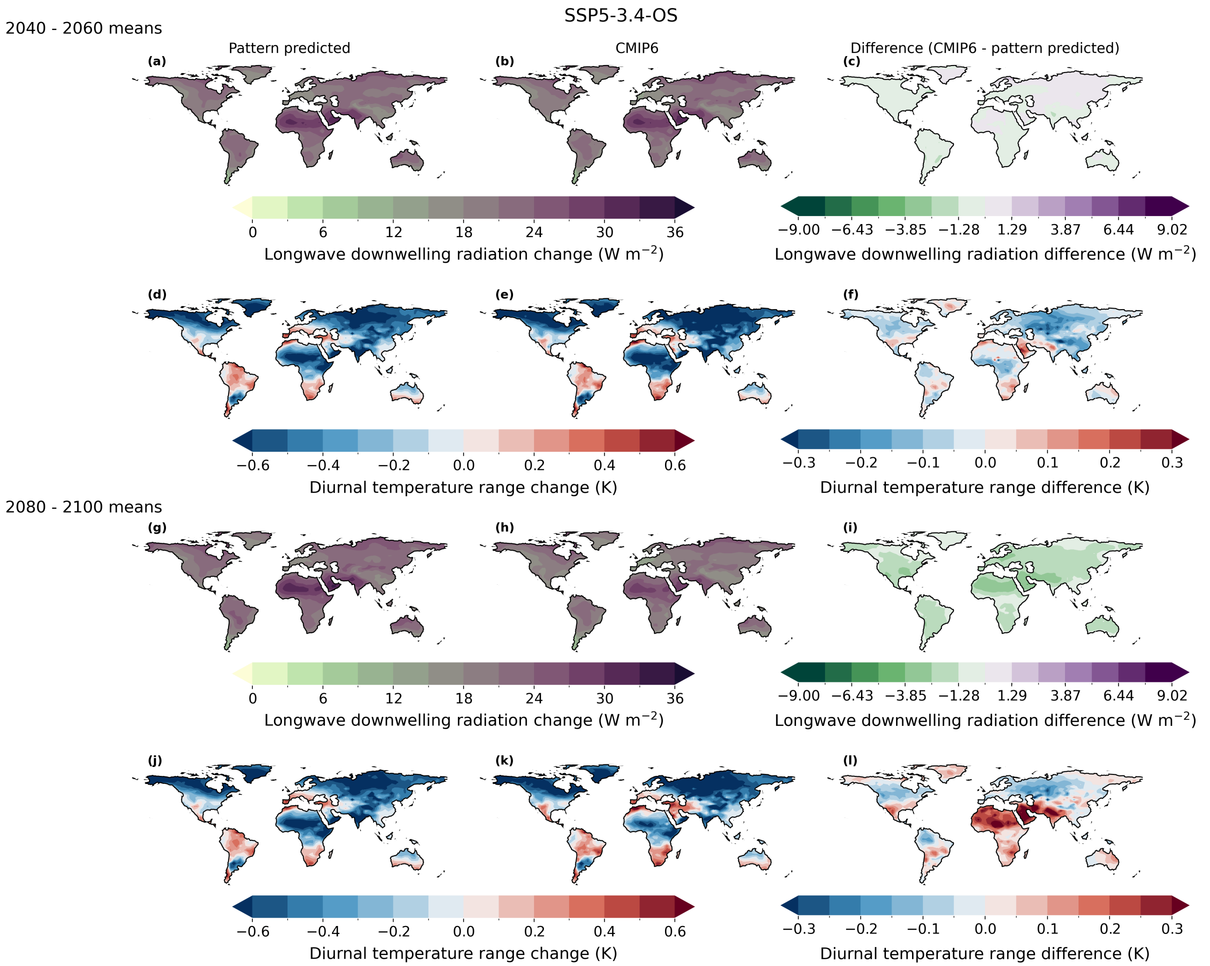

Figure S8. Evaluation of the pattern predicted ensemble mean anomalies compared to the CMIP6 ensemble mean anomalies for longwave downwelling radiation **(a-c, g-i)** and diurnal temperature range **(d-f, j-l)** for SSP5-3.4-OS. Maps **(a-f)** highlight mid-century predictions, and **(g-l)** show those for the end of century. The right hand column shows the difference between the predictions (left hand column) and CMIP6 (middle column). The colourbar for the differences is not the same as that for the anomalies, in order to show the detail in the prediction error, which is small compared to the change induced by the scenario.

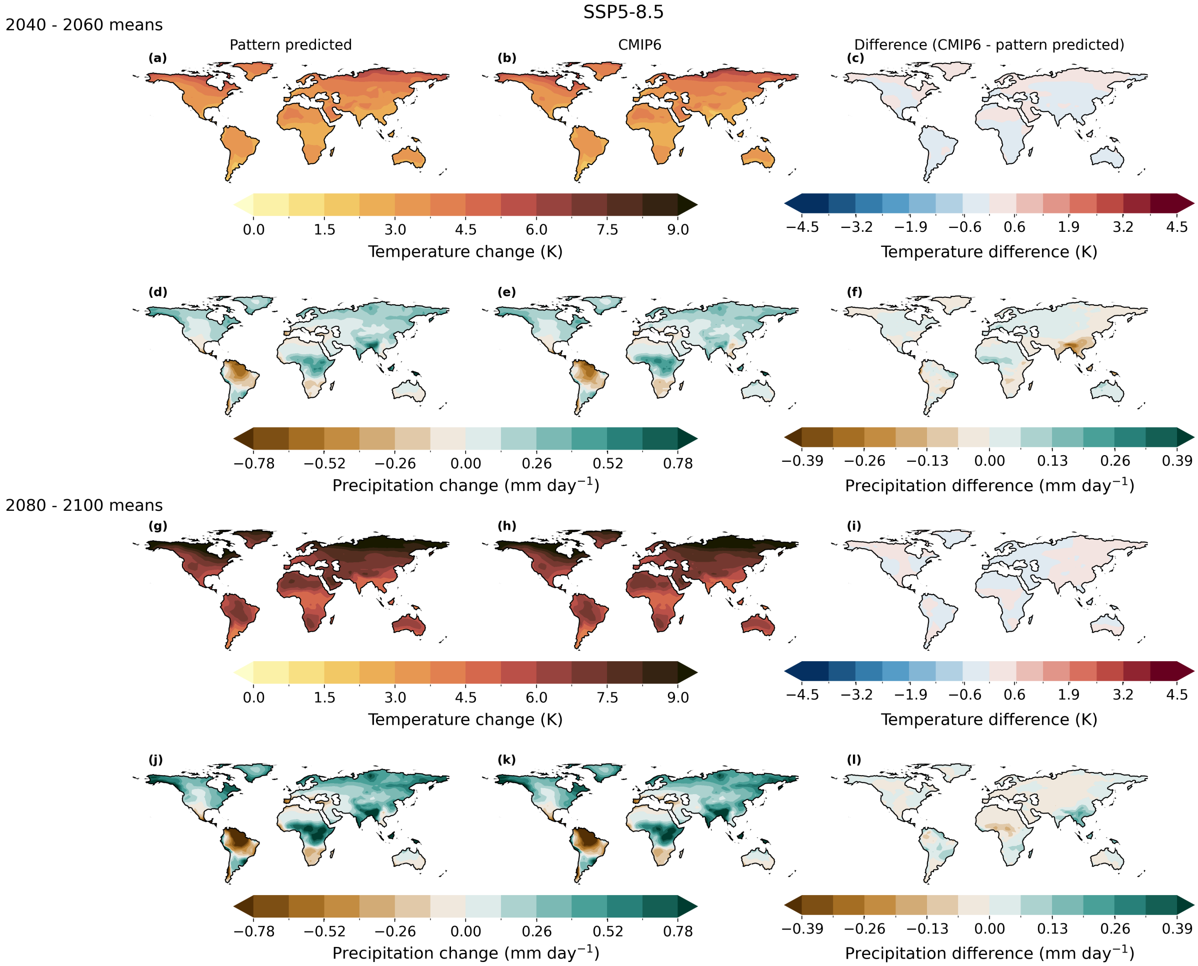

Figure S9. Evaluation of the pattern predicted ensemble mean anomalies compared to the CMIP6 ensemble mean anomalies for temperature **(a-c, g-i)** and precipitation **(d-f, j-l)** for SSP5-8.5, the training scenario. Maps **(a-f)** highlight mid-century predictions, and **(g-l)** show those for the end of century. The right hand column shows the difference between the predictions (left hand column) and CMIP6 (middle column). The colourbar for the differences is not the same as that for the anomalies, in order to show the detail in the prediction error, which is small compared to the change induced by the scenario.

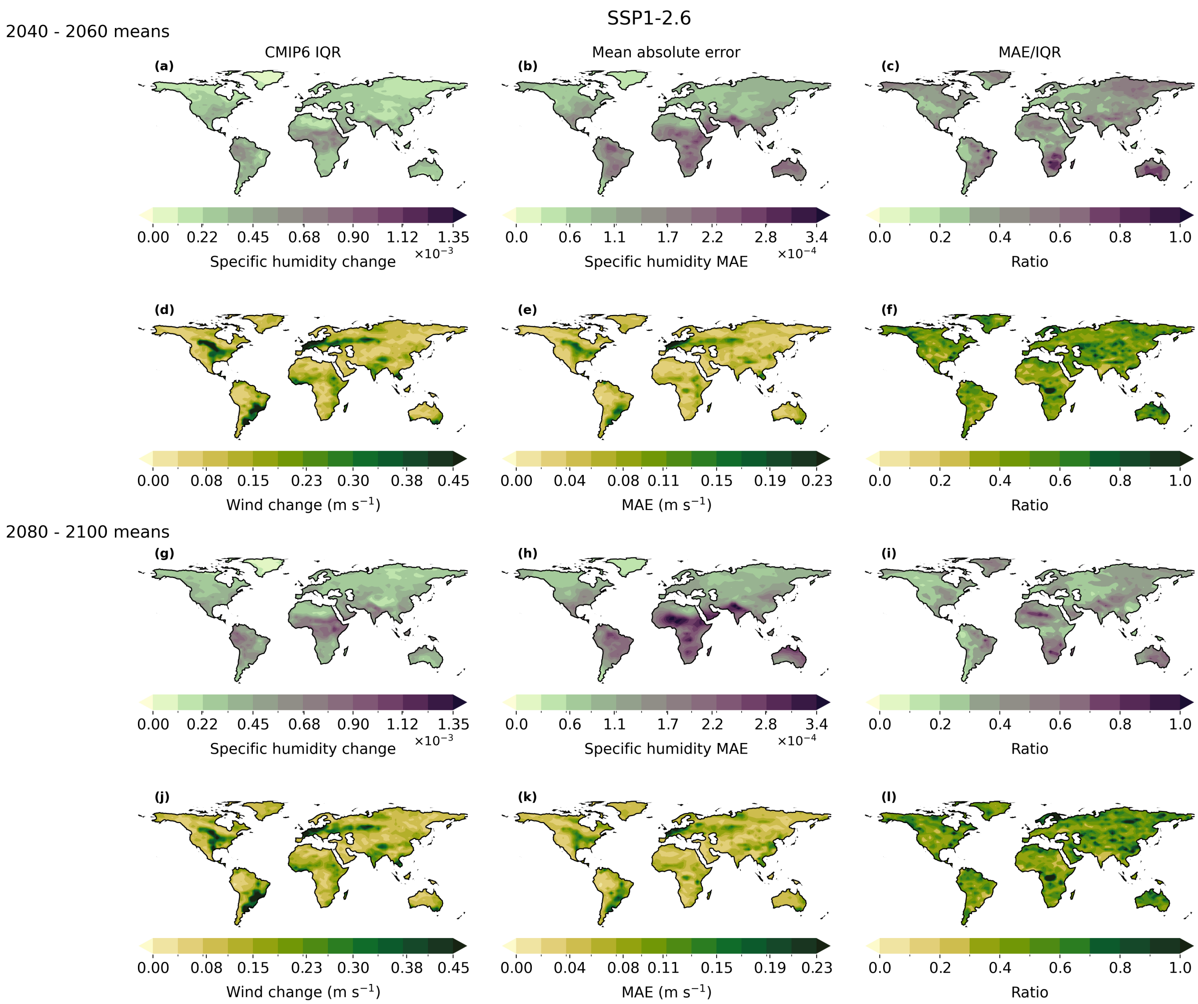

Figure S10. Evaluation of the interquartile range (IQR) of predictions (left column) and of the mean absolute model-to-model error (MAE) for specific humidity **(a-c, g-i)** and wind **(d-f, j-l)** for SSP1-2.6. Maps **(a-f)** highlight mid-century predictions, and **(g-l)** show those for the end of century. The middle column shows the MAE and the right hand column the ratio of MAE to IQR.

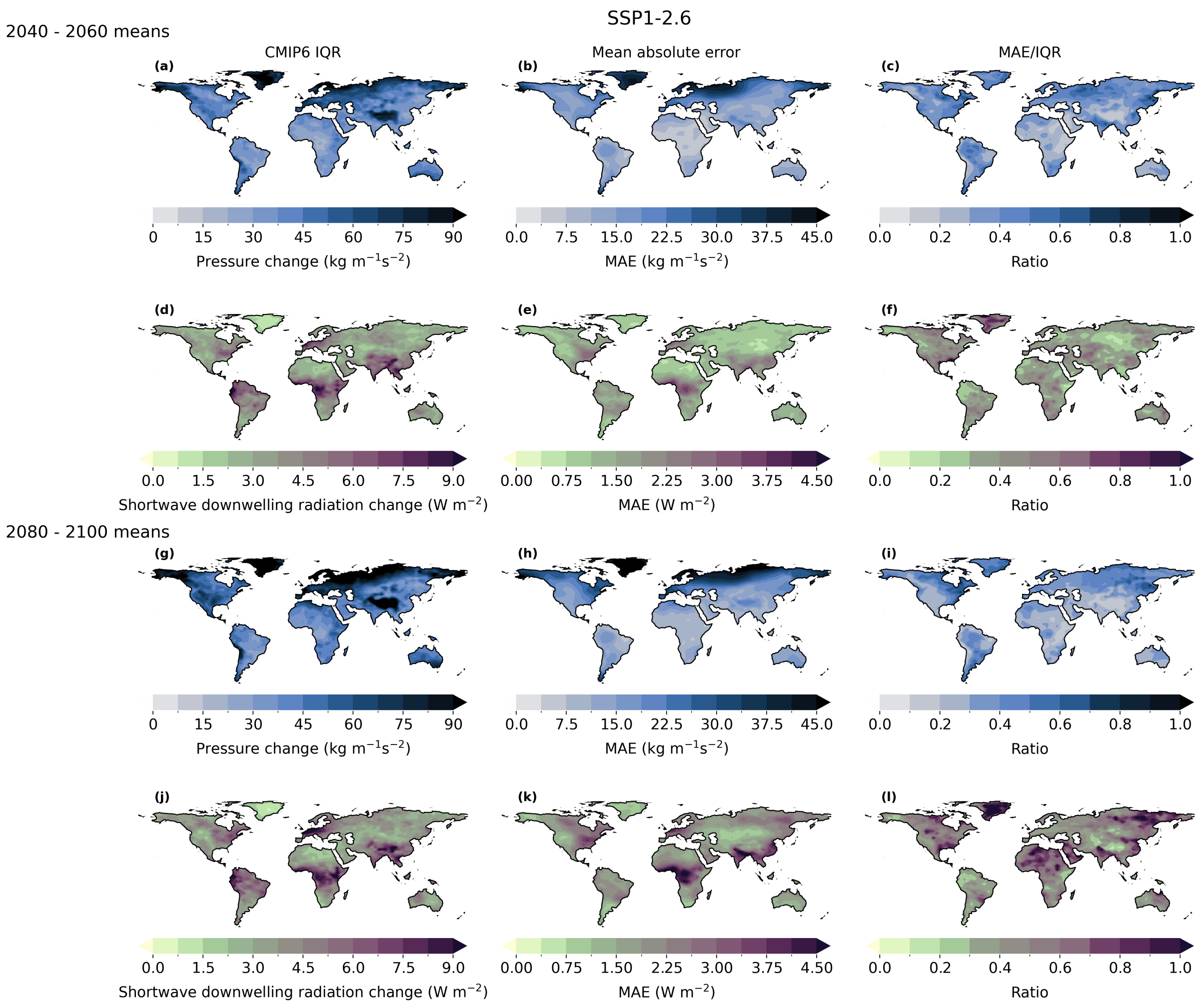

Figure S11. Evaluation of the interquartile range (IQR) of predictions (left column) and of the mean absolute model-to-model error (MAE) for pressure **(a-c, g-i)** and Shortwave downward radiation **(d-f, j-l)** for SSP1-2.6. Maps **(a-f)** highlight mid-century predictions, and **(g-l)** show those for the end of century. The middle column shows the MAE and the right hand column the ratio of MAE to IQR.

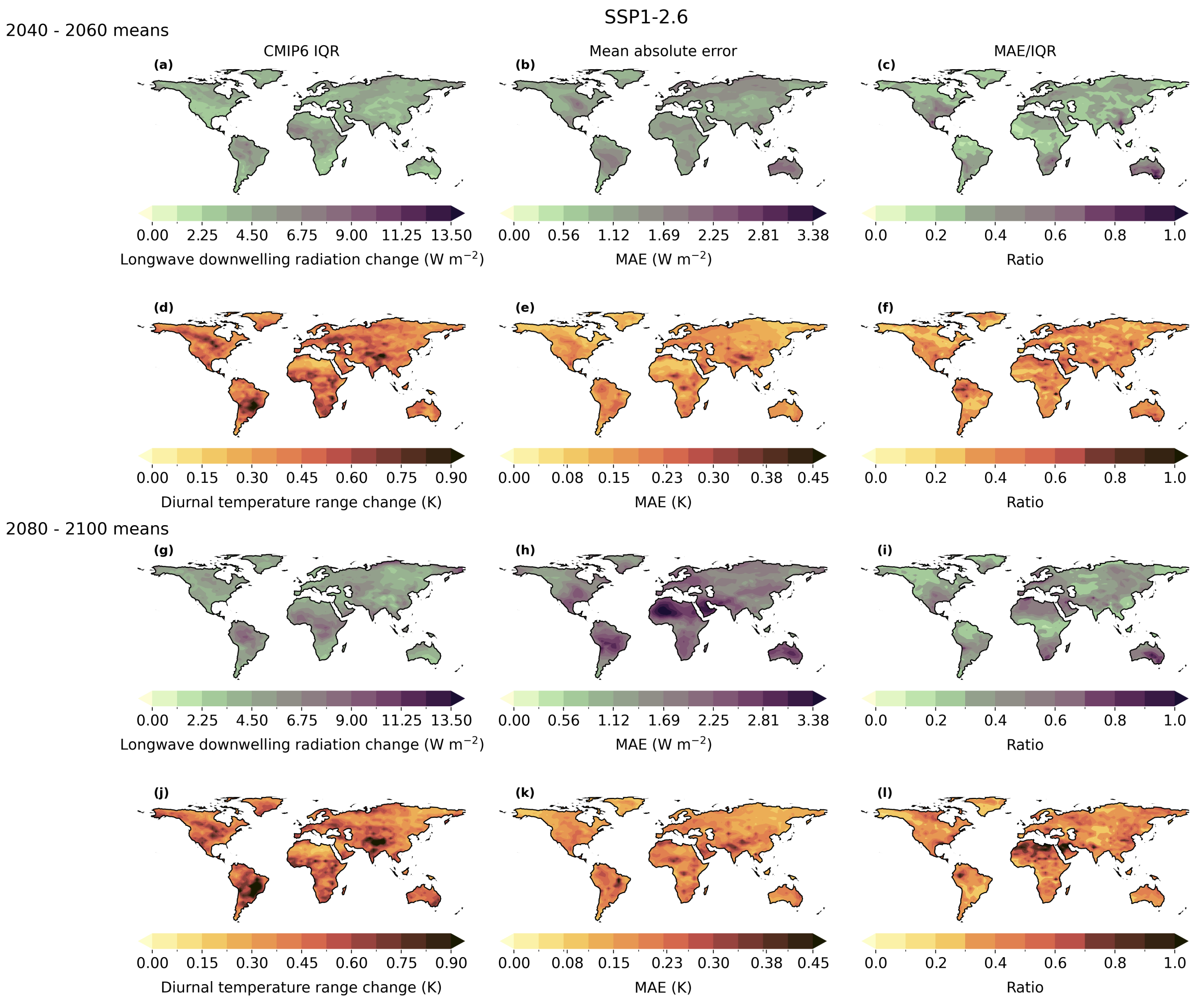

Figure S12. Evaluation of the interquartile range (IQR) of predictions (left column) and of the mean absolute model-to-model error (MAE) for longwave downwelling radiation **(a-c, g-i)** and diurnal temperature range **(d-f, j-l)** for SSP1-2.6. Maps **(a-f)** highlight mid-century predictions, and **(g-l)** show those for the end of century. The middle column shows the MAE and the right hand column the ratio of MAE to IQR.

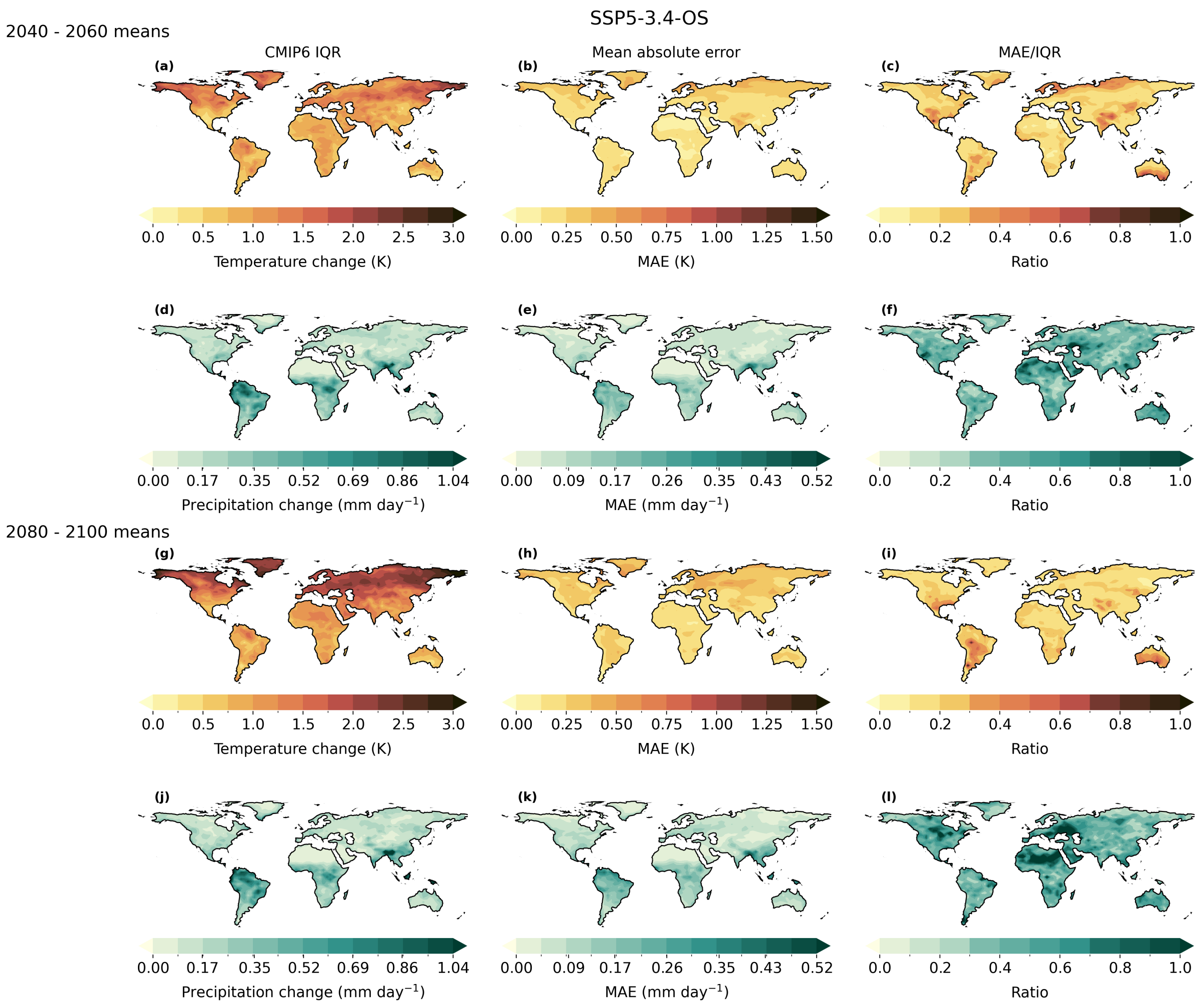

Figure S13. Evaluation of the interquartile range (IQR) of predictions (left column) and of the mean absolute model-to-model error (MAE) for temperature **(a-c, g-i)** and precipitation **(d-f, j-l)** for SSP5-3.4-OS. Maps **(a-f)** highlight mid-century predictions, and **(g-l)** show those for the end of century. The middle column shows the MAE and the right hand column the ratio of MAE to IQR.

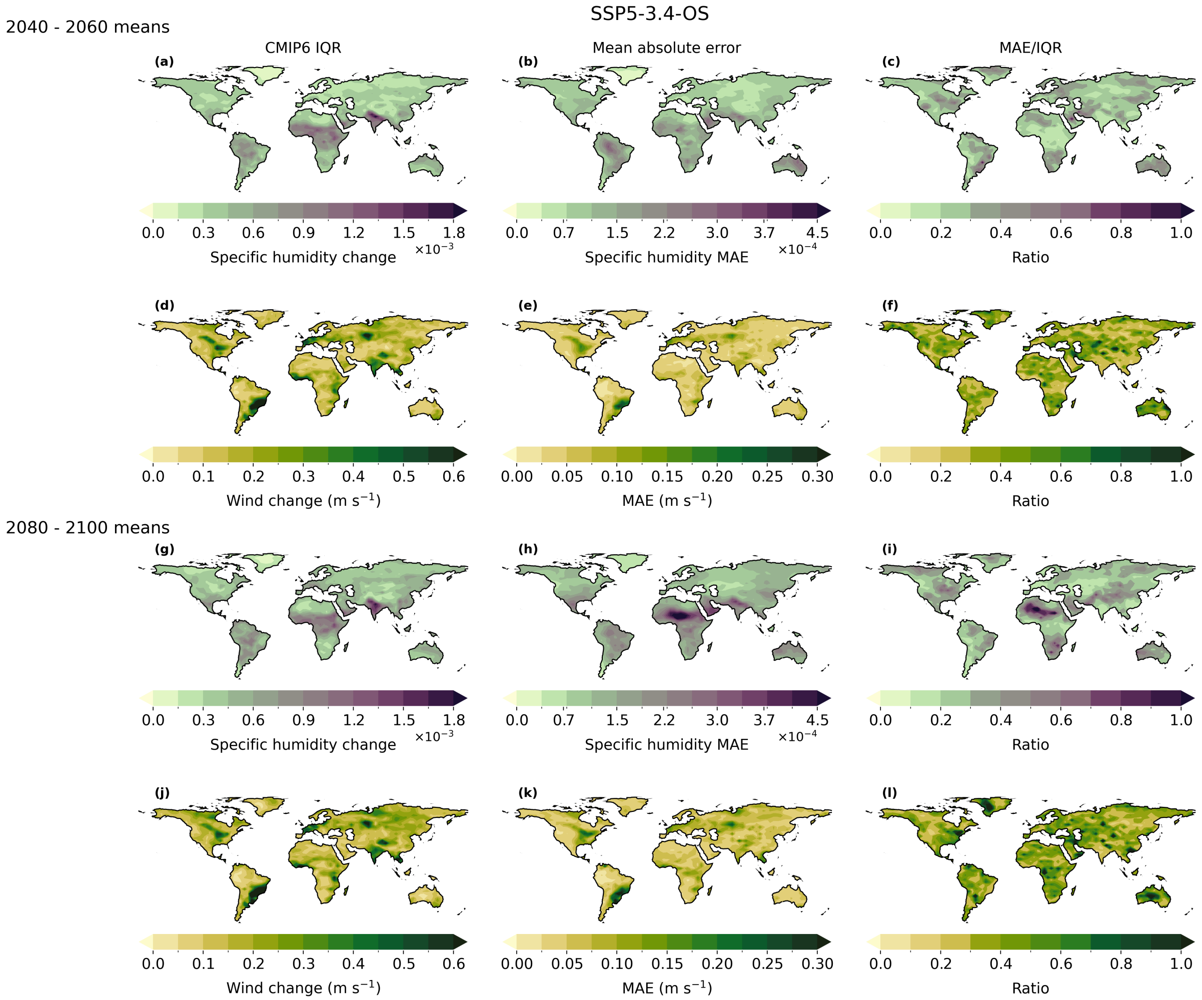

Figure S14. Evaluation of the interquartile range (IQR) of predictions (left column) and of the mean absolute model-to-model error (MAE) for specific humidity **(a-c, g-i)** and wind **(d-f, j-l)** for SSP5-3.4-OS. Maps **(a-f)** highlight mid-century predictions, and **(g-l)** show those for the end of century.The middle column shows the MAE and the right hand column the ratio of MAE to IQR.

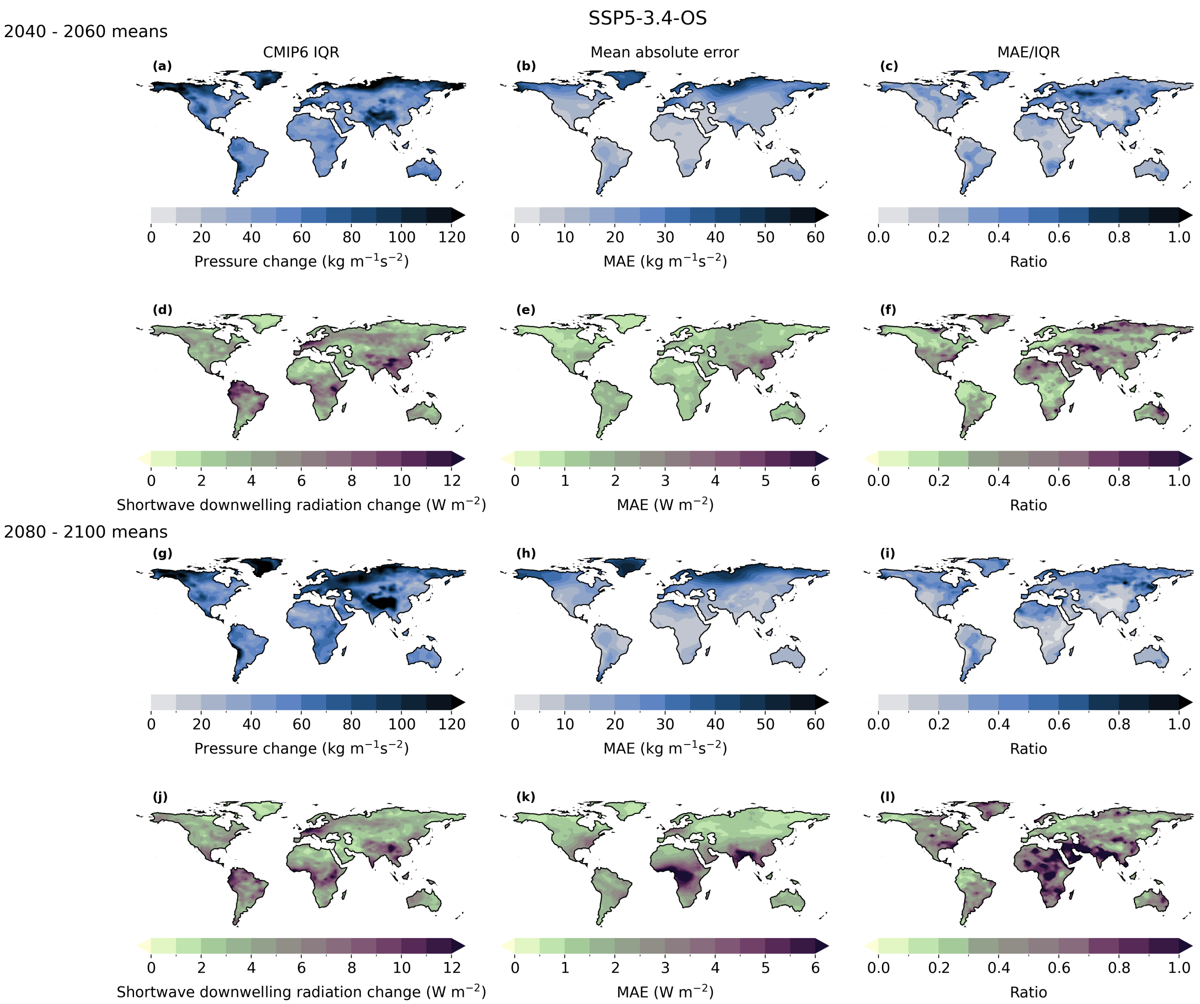

Figure S15. Evaluation of the interquartile range (IQR) of predictions (left column) and of the mean absolute model-to-model error (MAE) for pressure **(a-c, g-i)** and Shortwave downward radiation **(d-f, j-l)** for SSP5-3.4-OS. Maps **(a-f)** highlight mid-century predictions, and **(g-l)** show those for the end of century. The middle column shows the MAE and the right hand column the ratio of MAE to IQR.

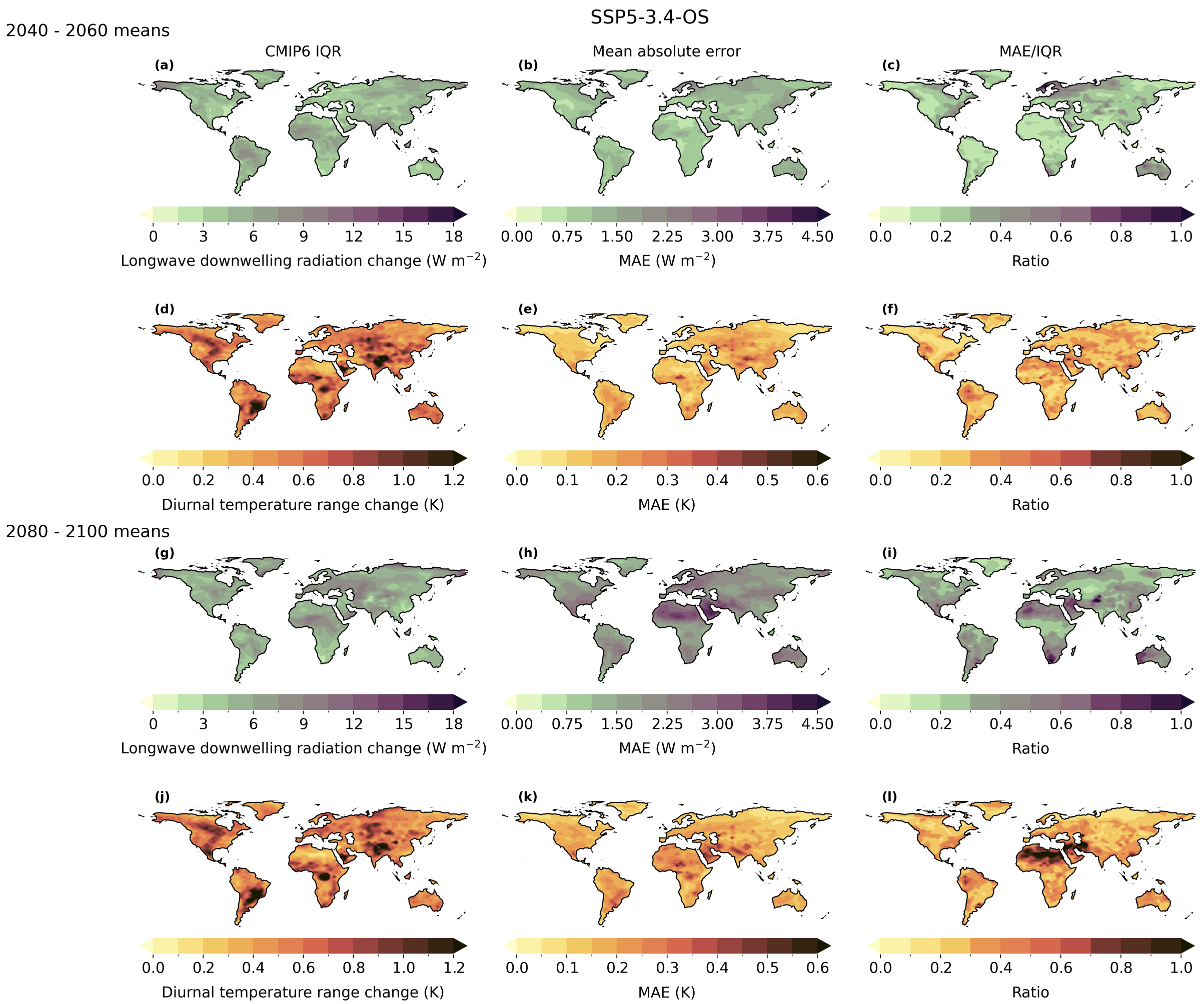

Figure S16. Evaluation of the interquartile range (IQR) of predictions (left column) and of the mean absolute model-to-model error (MAE) for longwave downwelling radiation **(a-c, g-i)** and diurnal temperature range **(d-f, j-l)** for SSP5-3.4-OS. Maps **(a-d)** highlight mid-century predictions, and **(e-h)** show those for the end of century.The middle column shows the MAE and the right hand column the ratio of MAE to IQR.

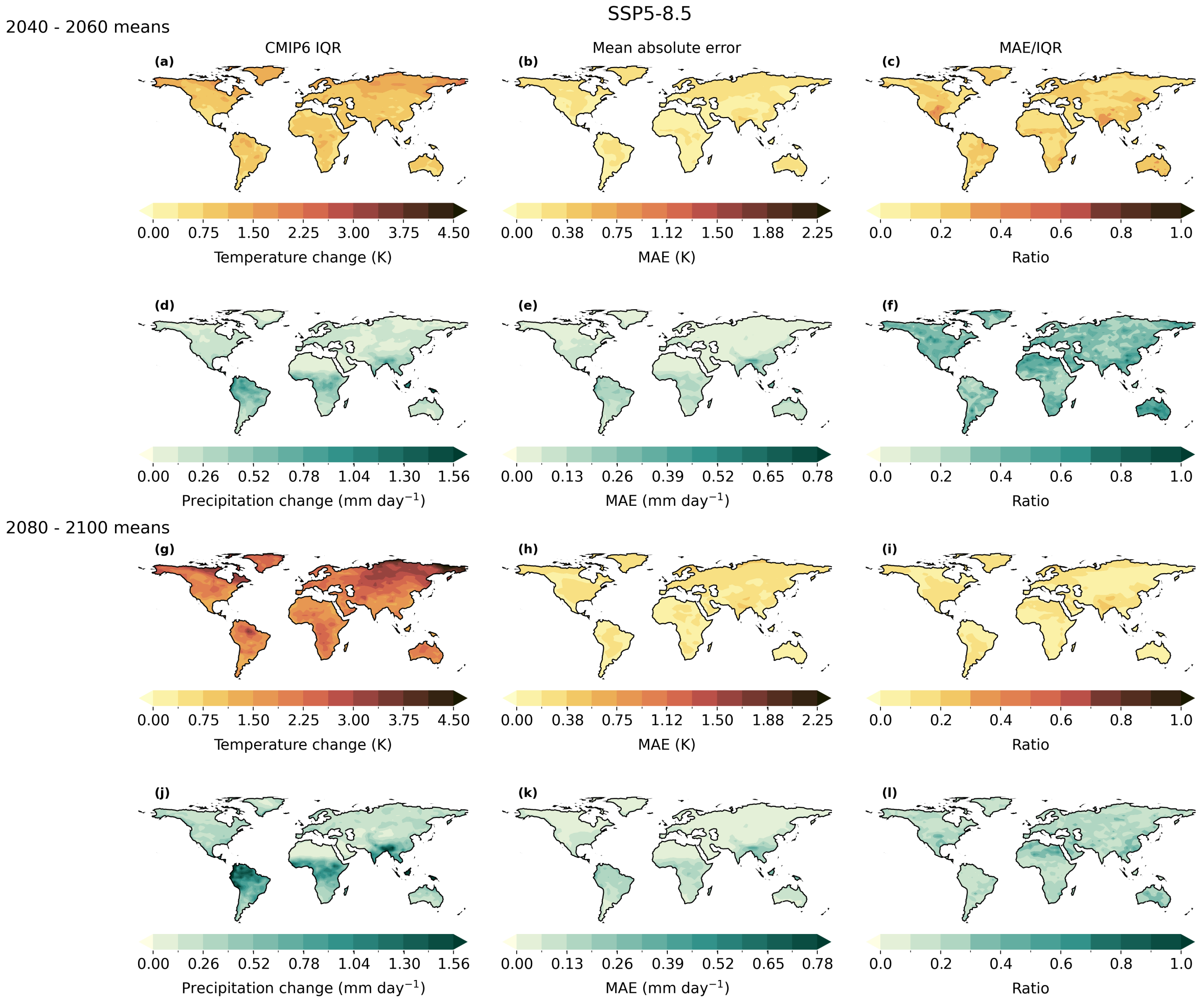

Figure S17. Evaluation of the interquartile range (IQR) of predictions (left column) and of the mean absolute model-to-model error (MAE) for temperature **(a-c, g-i)** and precipitation **(d-f, j-l)** for SSP5-8.5, the training scenario. Maps **(a-d)** highlight mid-century predictions, and **(e-h)** show those for the end of century. The middle column shows the MAE and the right hand column the ratio of MAE to IQR.

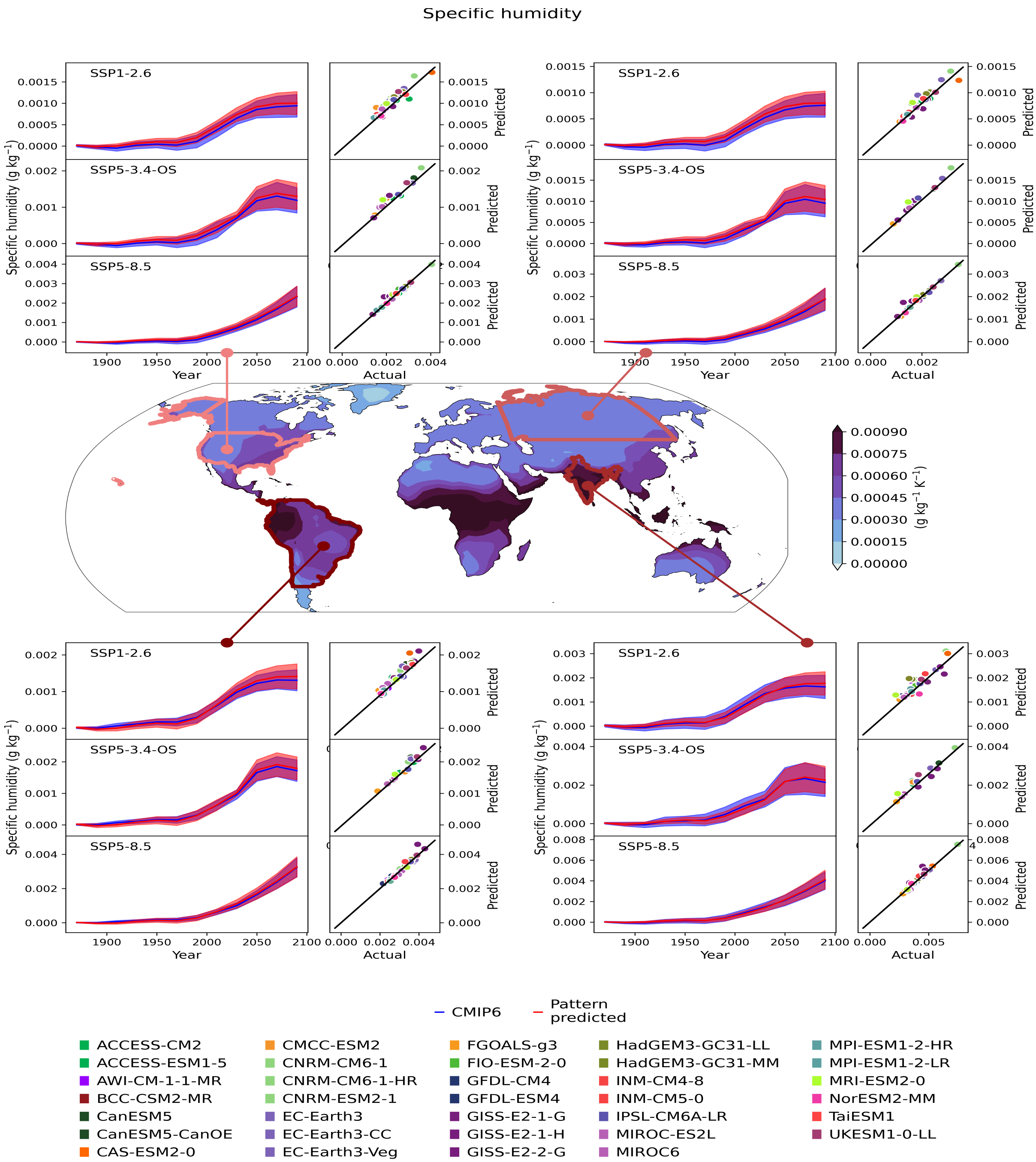

Figure S18. The central map shows the specific humidity pattern (where there is no hatching indicates that the models tend to agree on the sign of the change and with hatching to show where the models tend to disagree on the sign of the change), and subpanels for each region: North America, Siberia, South America and South Asia. The region subpanels show the specific humidity timeseries (left subpanel) and scatter plots (right subpanel) for each scenario; top: SSP1-2.6, middle: SSP5-3.4-OS and bottom: S5P-8.5, the training scenario. The timeseries shows the PRIME patterns (blue plume) and the CMIP6 patterns (red plume). The scatter plots show the end of century values predicted by PRIME vs CMIP6 actual values for each model with the model colours shown at the bottom of the figure.

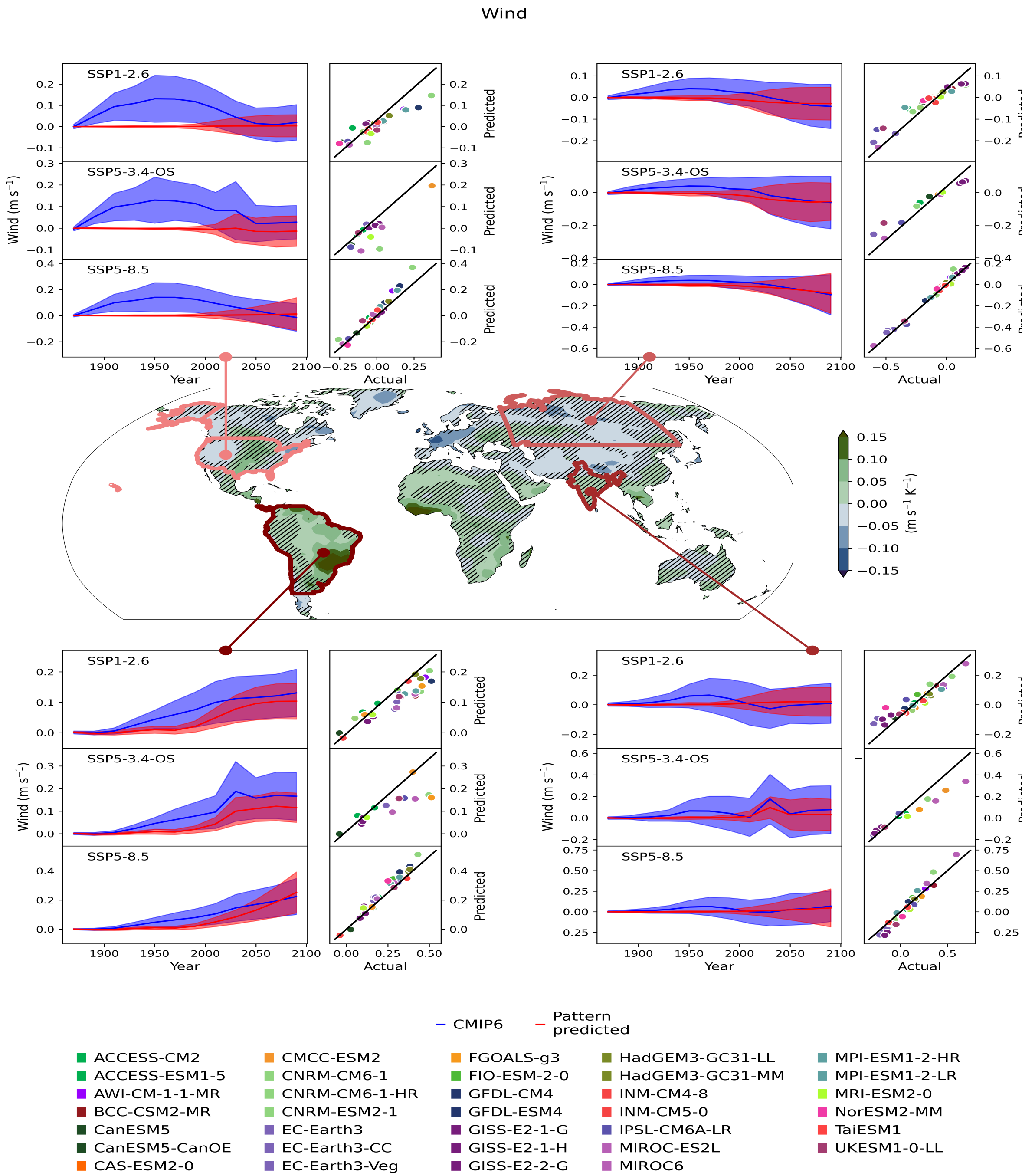

Figure S19. The central map shows the wind pattern (where there is no hatching indicates that the models tend to agree on the sign of the change and with hatching to show where the models tend to disagree on the sign of the change) and subpanels for each region: North America, Siberia, South America and South Asia. The region subpanels show the wind timeseries (left subpanel) and scatter plots (right subpanel) for each scenario; top: SSP1-2.6, middle: SSP5-3.4-OS and bottom: SSP5-8.5, the training scenario. The timeseries shows the PRIME patterns (blue plume) and the CMIP6 patterns (red plume). The scatter plots show the end of century values predicted by PRIME vs CMIP6 actual values for each model with the model colours shown at the bottom of the figure.

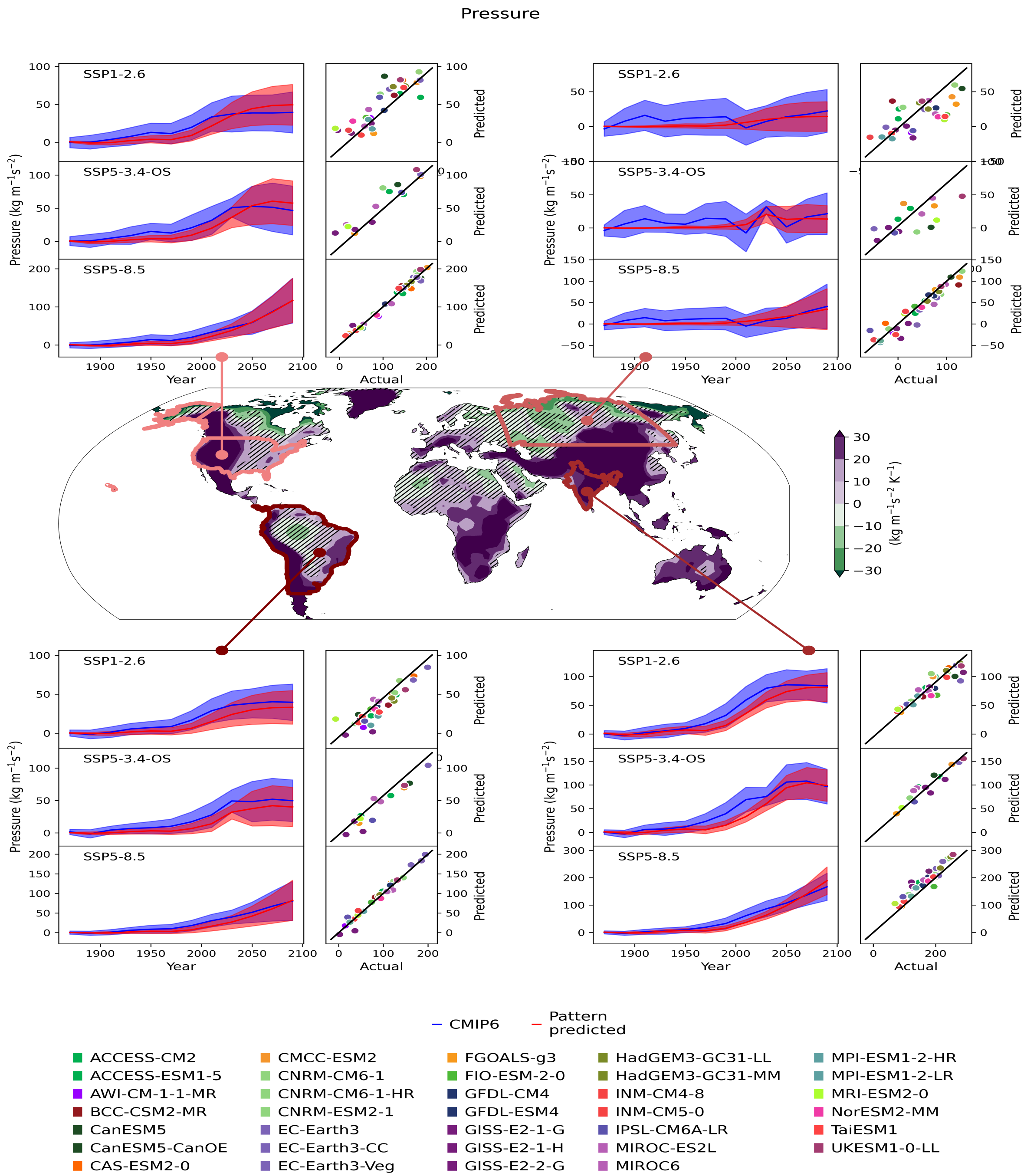

Figure S20. The central map shows the pressure pattern (where there is no hatching indicates that the models tend to agree on the sign of the change and with hatching to show where the models tend to disagree on the sign of the change) and subpanels for each region: North America, Siberia, South America and South Asia. The region subpanels show the pressure timeseries (left subpanel) and scatter plots (right subpanel) for each scenario; top: SSP1-2.6, middle: SSP5-3.4-OS and bottom: SSP5-8.5, the training scenario. The timeseries shows the PRIME patterns (blue plume) and the CMIP6 patterns (red plume). The scatter plots show the end of century values predicted by PRIME vs CMIP6 actual values for each model with the model colours shown at the bottom of the figure.

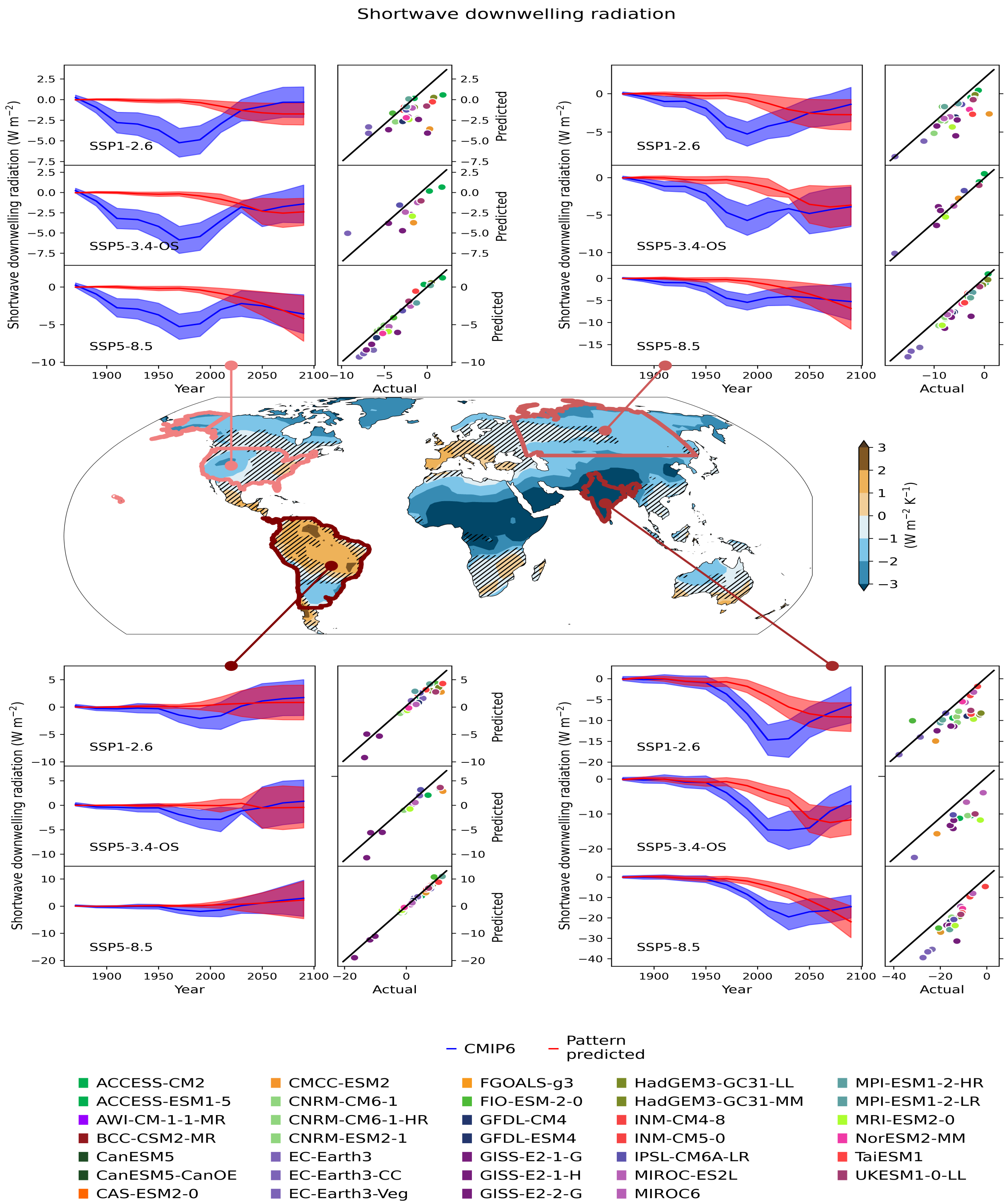

Figure S21. The central map shows the shortwave downward radiation pattern (where there is no hatching indicates that the models tend to agree on the sign of the change and with hatching to show where the models tend to disagree on the sign of the change) and subpanels for each region: North America, Siberia, South America and South Asia. The region subpanels show the shortwave downward radiation timeseries (left subpanel) and scatter plots (right subpanel) for each scenario; top: SSP1-2.6, middle: SSP5-3.4-OS and bottom: SSP5-8.5, the training scenario. The timeseries shows the PRIME patterns (blue plume) and the CMIP6 patterns (red plume). The scatter plots show the end of century values predicted by PRIME vs CMIP6 actual values for each model with the model colours shown at the bottom of the figure.

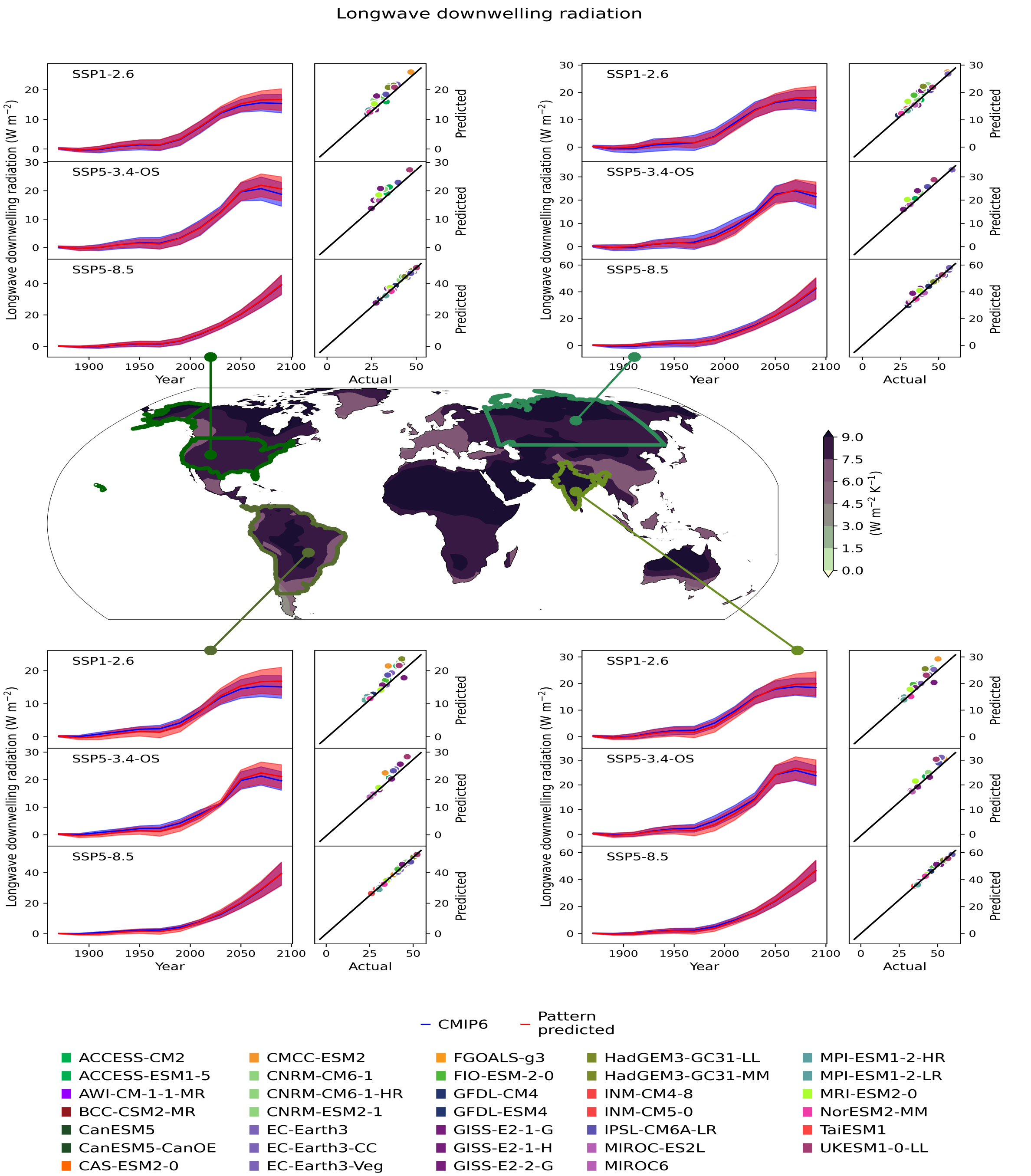

Figure S22. The central map shows the longwave downward radiation pattern (where there is no hatching indicates that the models tend to agree on the sign of the change and with hatching to show where the models tend to disagree on the sign of the change) and subpanels for each region: North America, Siberia, South America and South Asia. The region subpanels show the longwave downward radiation timeseries (left subpanel) and scatter plots (right subpanel) for each scenario; top: SSP1-2.6, middle: SSP5-3.4-OS and bottom: SSP5-8.5, the training scenario. The timeseries shows the PRIME patterns (blue plume) and the CMIP6 patterns (red plume). The scatter plots show the end of century values predicted by PRIME vs CMIP6 actual values for each model with the model colours shown at the bottom of the figure.

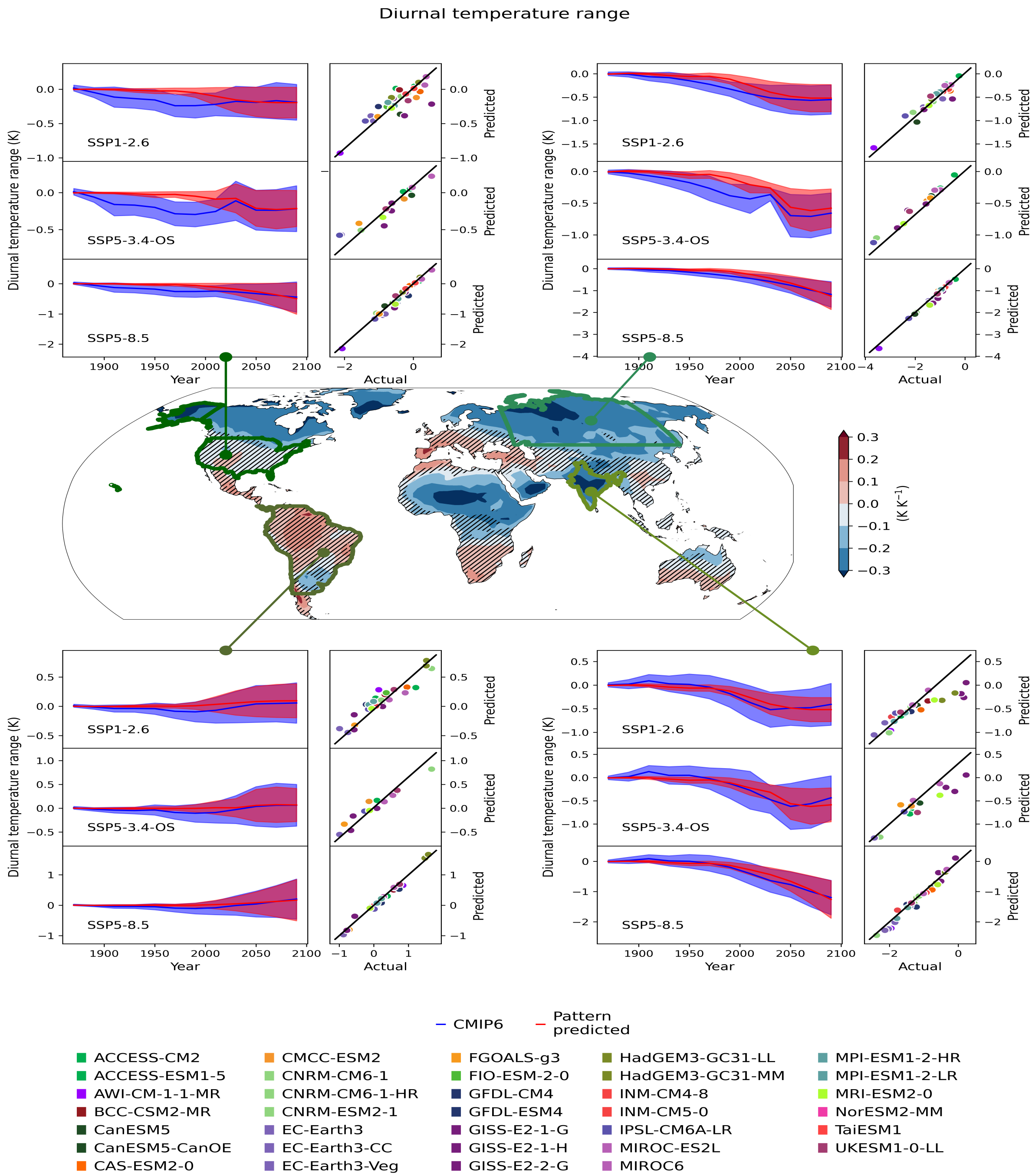

Figure S23. The central map shows the diurnal surface temperature range pattern (where there is no hatching indicates that the models tend to agree on the sign of the change and with hatching to show where the models tend to disagree on the sign of the change) and subpanels for each region: North America, Siberia, South America and South Asia. The region subpanels show the diurnal surface temperature range timeseries (left subpanel) and scatter plots (right subpanel) for each scenario; top: SSP1-2.6, middle: SSP5-3.4-OS and bottom: SSP5-8.5, the training scenario. The timeseries shows the PRIME patterns (blue plume) and the CMIP6 patterns (red plume). The scatter plots show the end of century values predicted by PRIME vs CMIP6 actual values for each model with the model colours shown at the bottom of the figure.

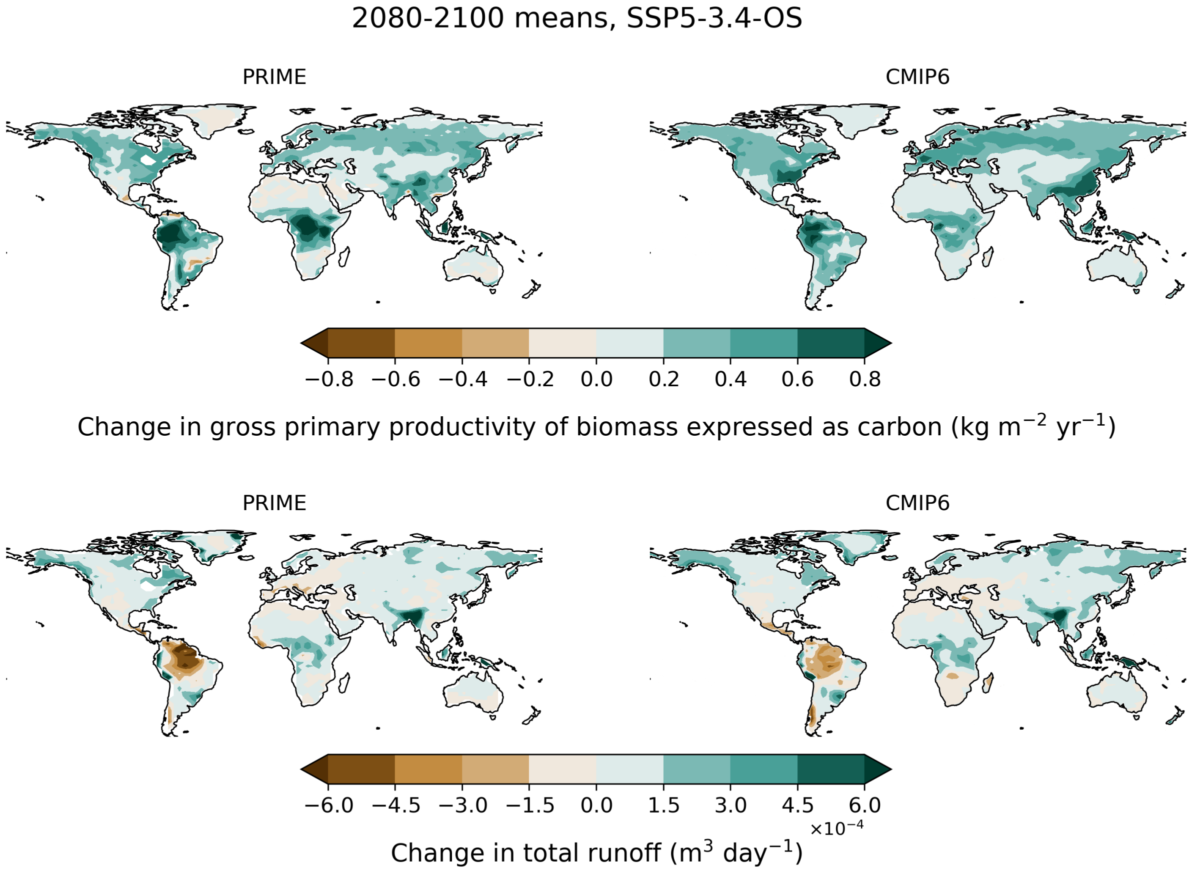

Figure S24. Maps comparing the multi-model mean projected end of century changes (2080–2100) for SSP5-3.4-OS for GPP (top) and runoff (bottom) from PRIME (left) compared to CMIP6 (right)

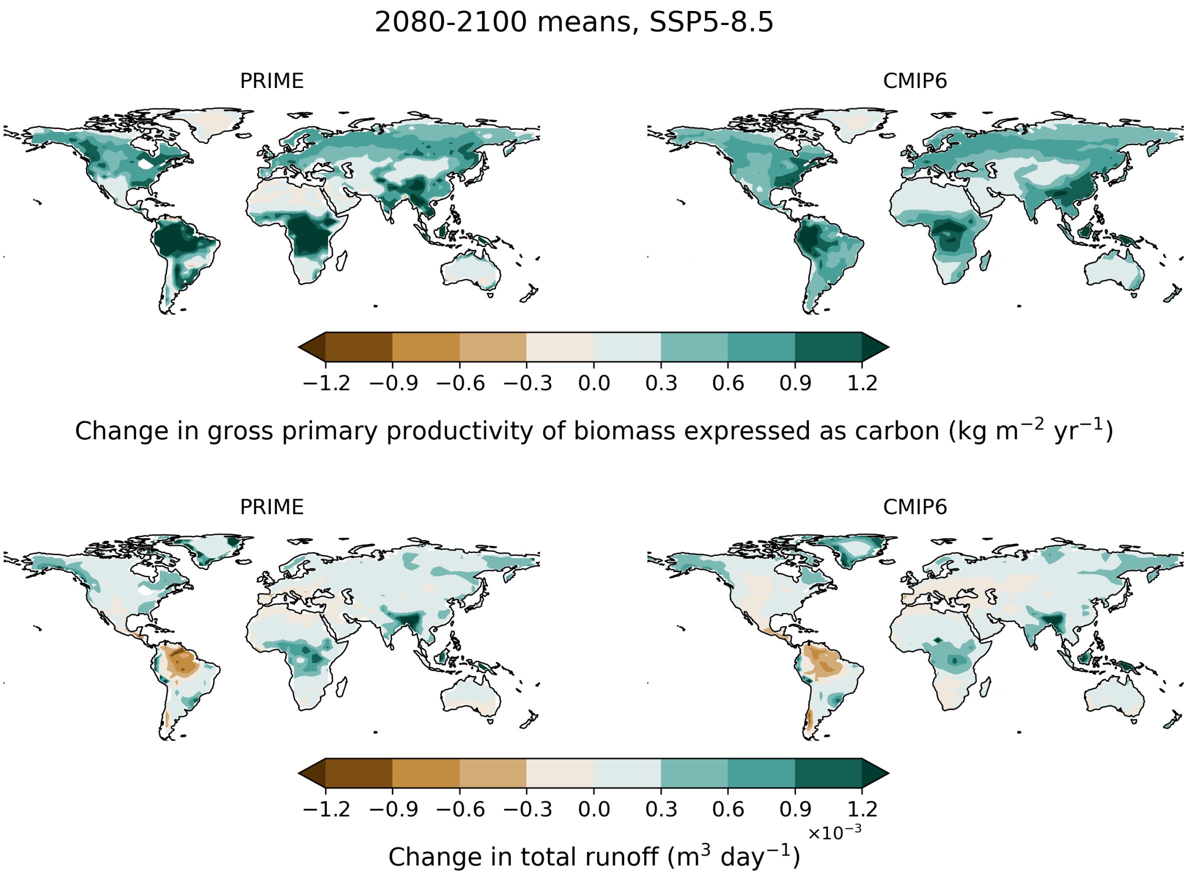

Figure S25. Maps comparing the multi-model mean projected end of century changes (2080–2100) for SSP5-8.5, the training scenario, for GPP (top) and runoff (bottom) from PRIME (left) compared to CMIP6 (right)

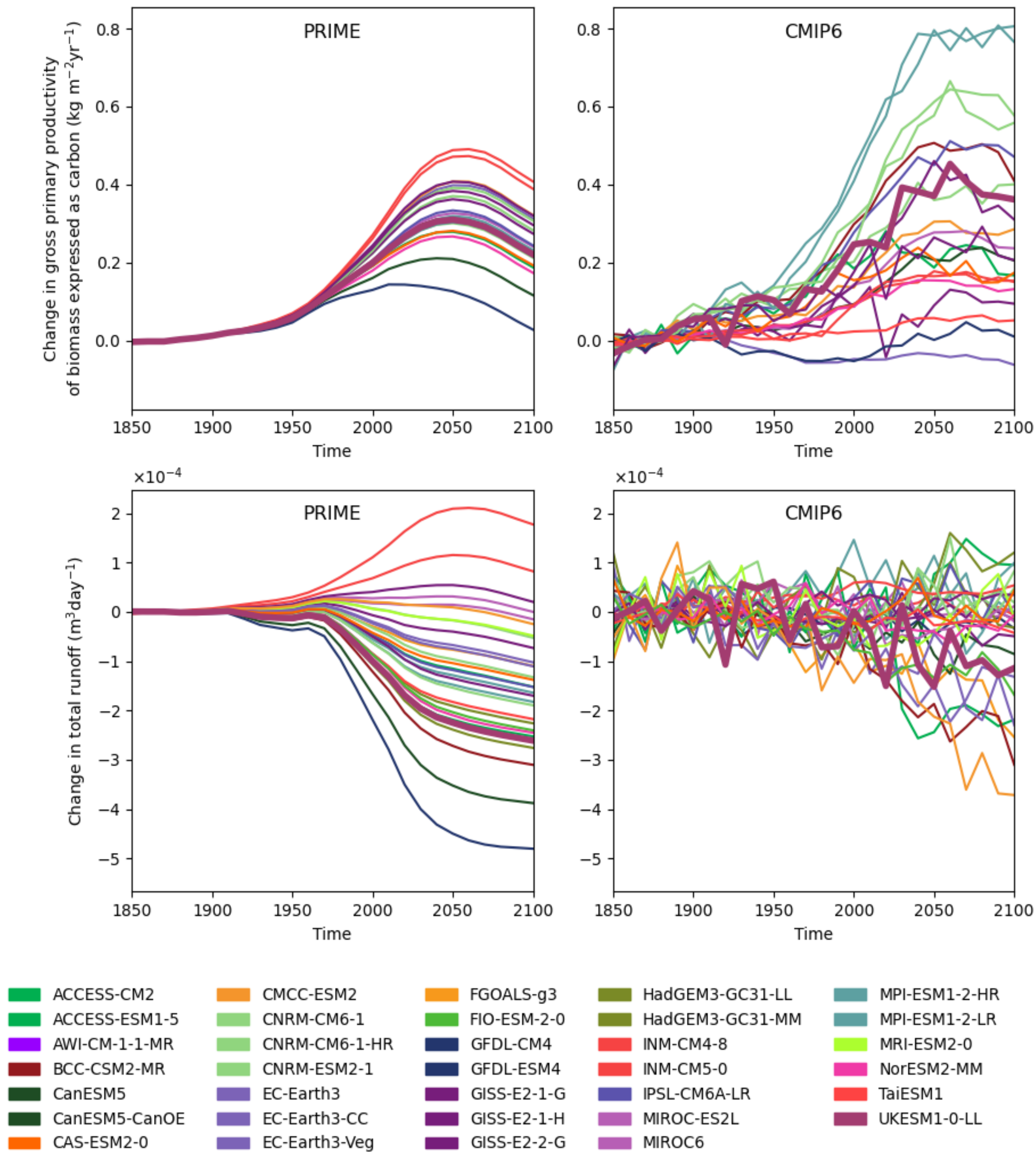

Figure S26. Timeseries of the change in gpp (top) and change in total runoff (bottom) for PRIME (left) and CMIP6 (right) for SSP1-2.6 for the South America region for each CMIP6 model

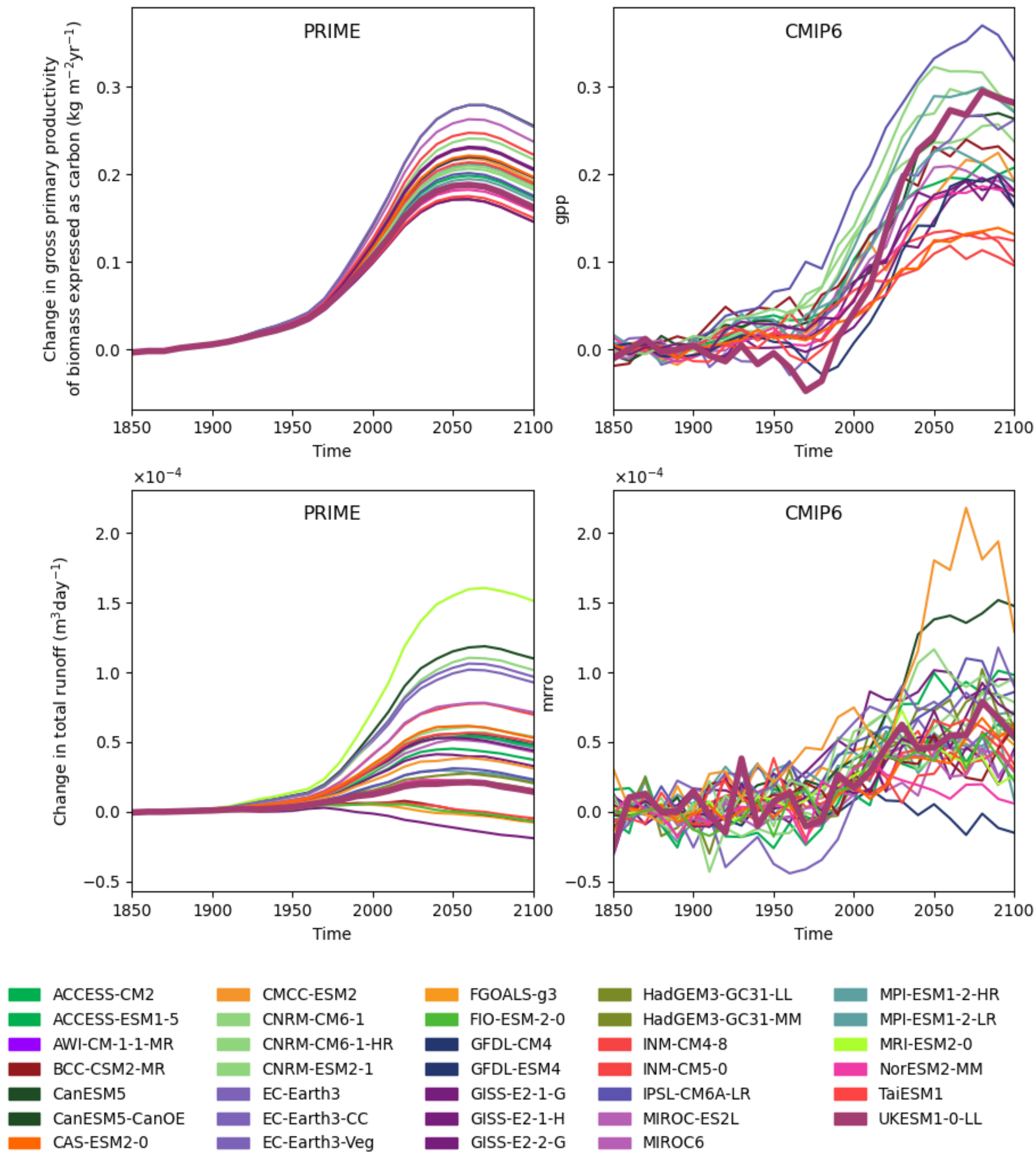

Figure S27. Timeseries of the change in gpp (top) and change in total runoff (bottom) for PRIME (left) and CMIP6 (right) for SSP1-2.6 for the Siberia region for each CMIP6 model

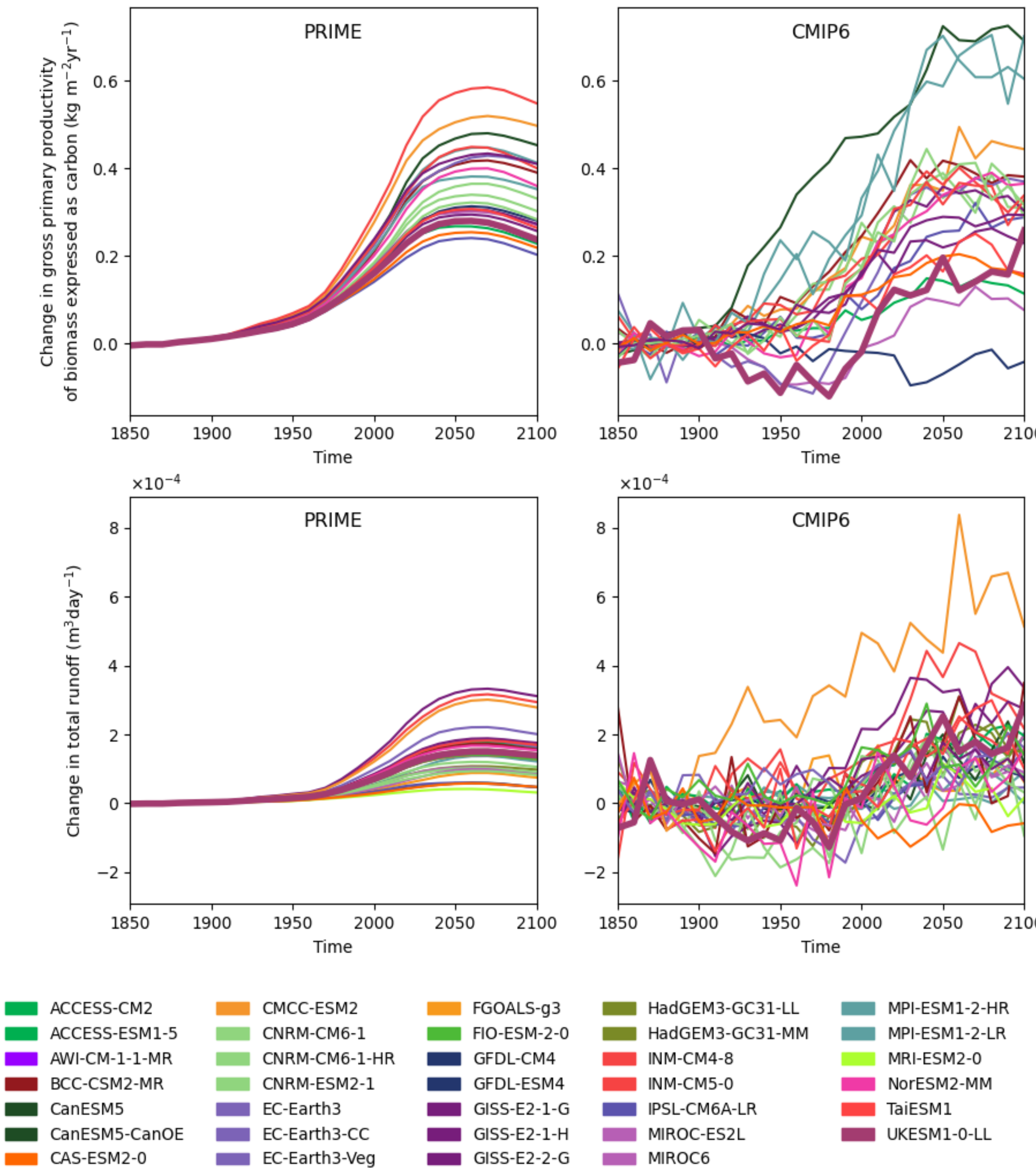

Figure S28. Timeseries of the change in gpp (top) and change in total runoff (bottom) for PRIME (left) and CMIP6 (right) for SSP1-2.6 for the India region for each CMIP6 model

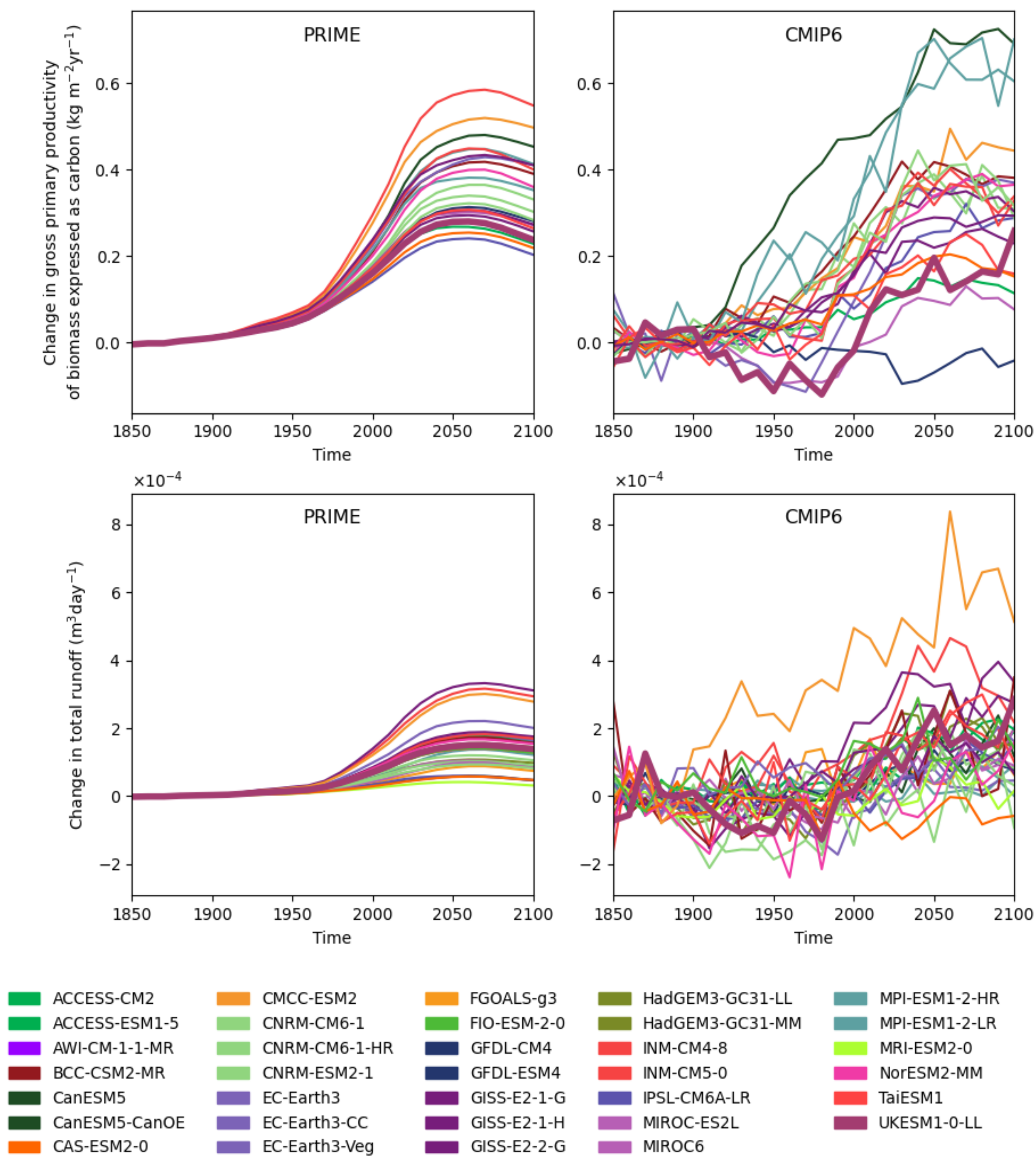

Figure S29. Timeseries of the change in gpp (top) and change in total runoff (bottom) for PRIME (left) and CMIP6 (right) for SSP1-2.6 for the USA region for each CMIP6 model

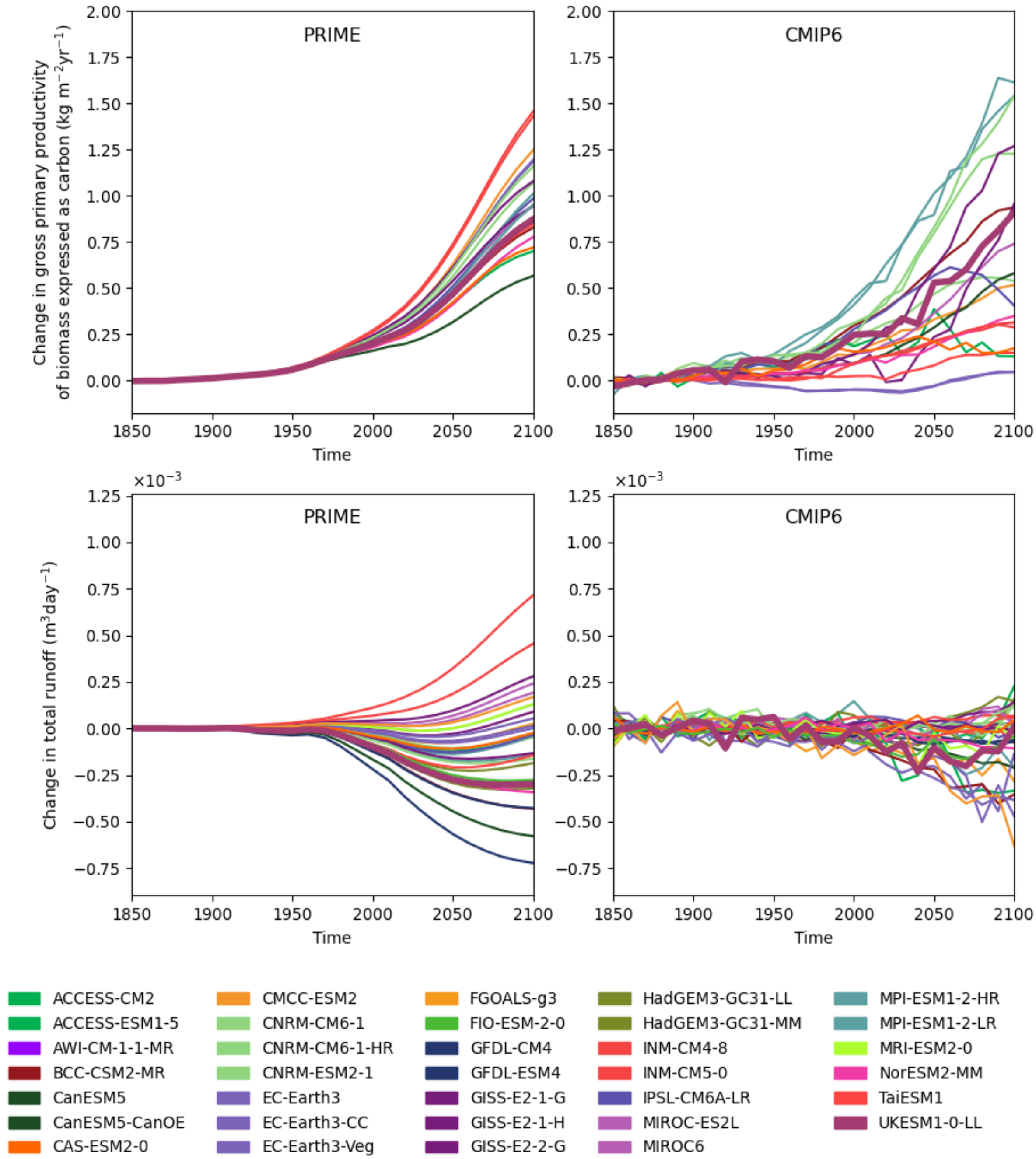

Figure S30. Timeseries of the change in gpp (top) and change in total runoff (bottom) for PRIME (left) and CMIP6 (right) for SSP5-8.5, the training scenario for the South America region for each CMIP6 model

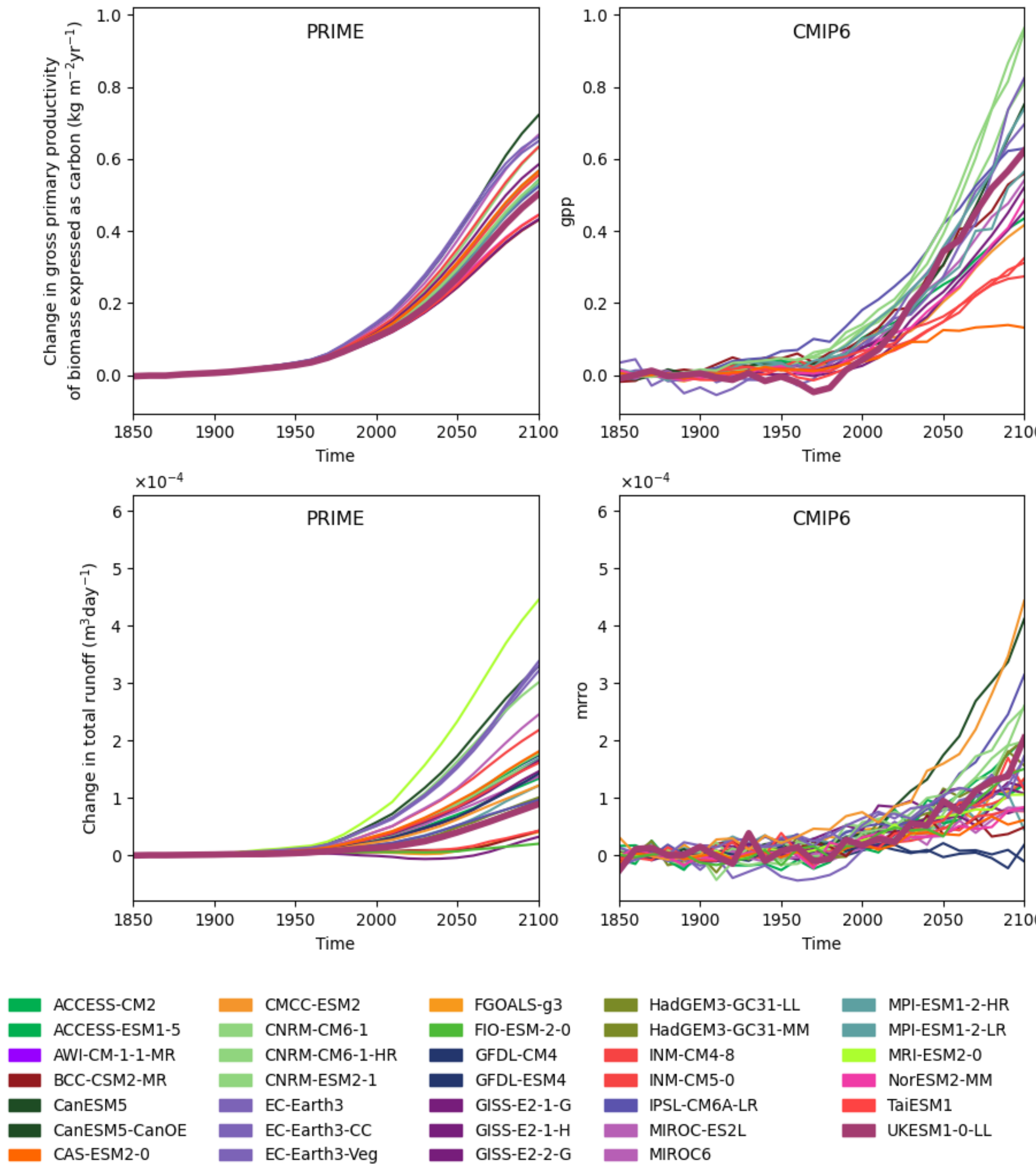

Figure S31. Timeseries of the change in gpp (top) and change in total runoff (bottom) for PRIME (left) and CMIP6 (right) for SSP5-8.5, the training scenario for the Siberia region for each CMIP6 model

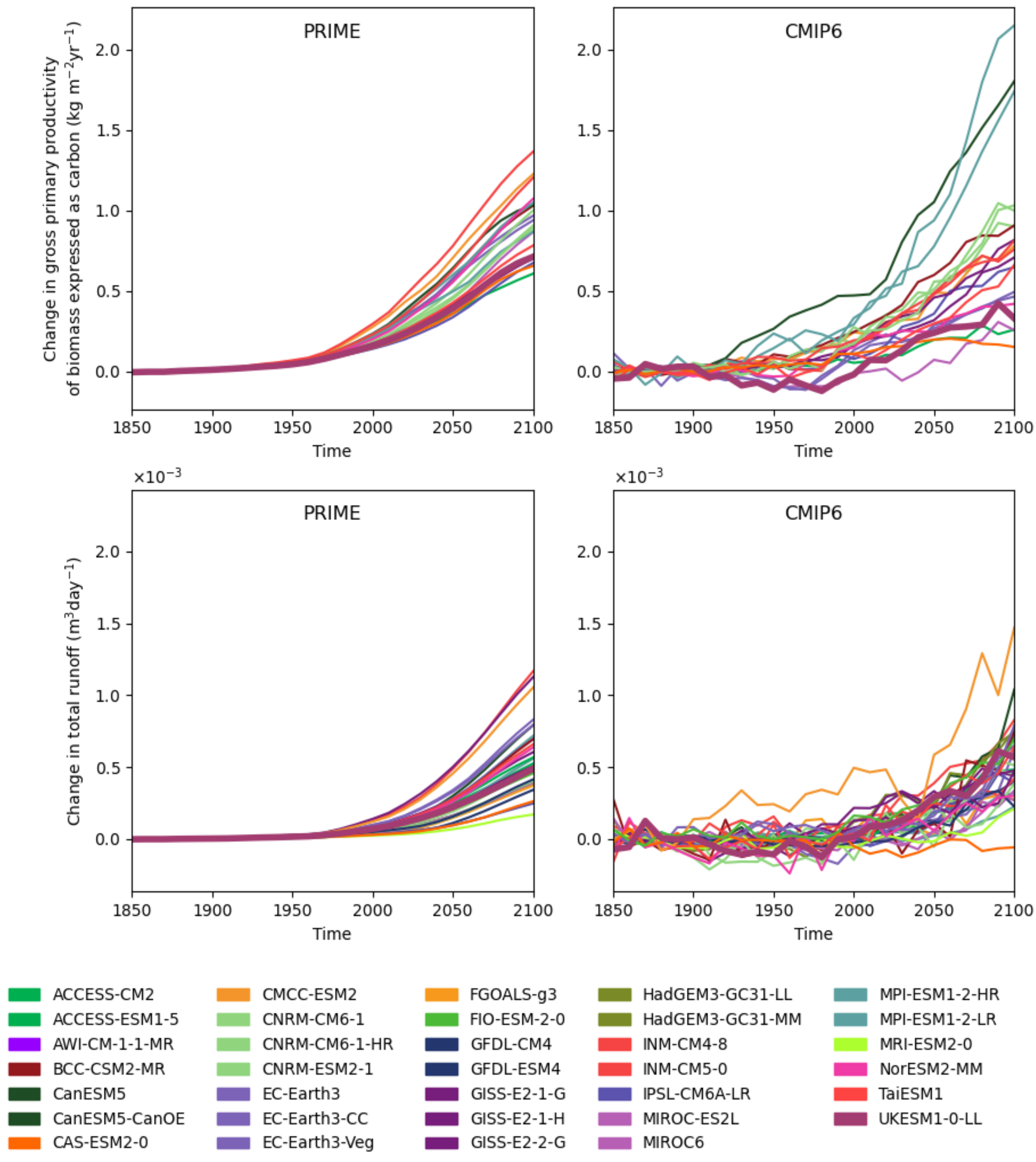

Figure S32. Timeseries of the change in gpp (top) and change in total runoff (bottom) for PRIME (left) and CMIP6 (right) for SSP5-8.5, the training scenario for the India region for each CMIP6 model

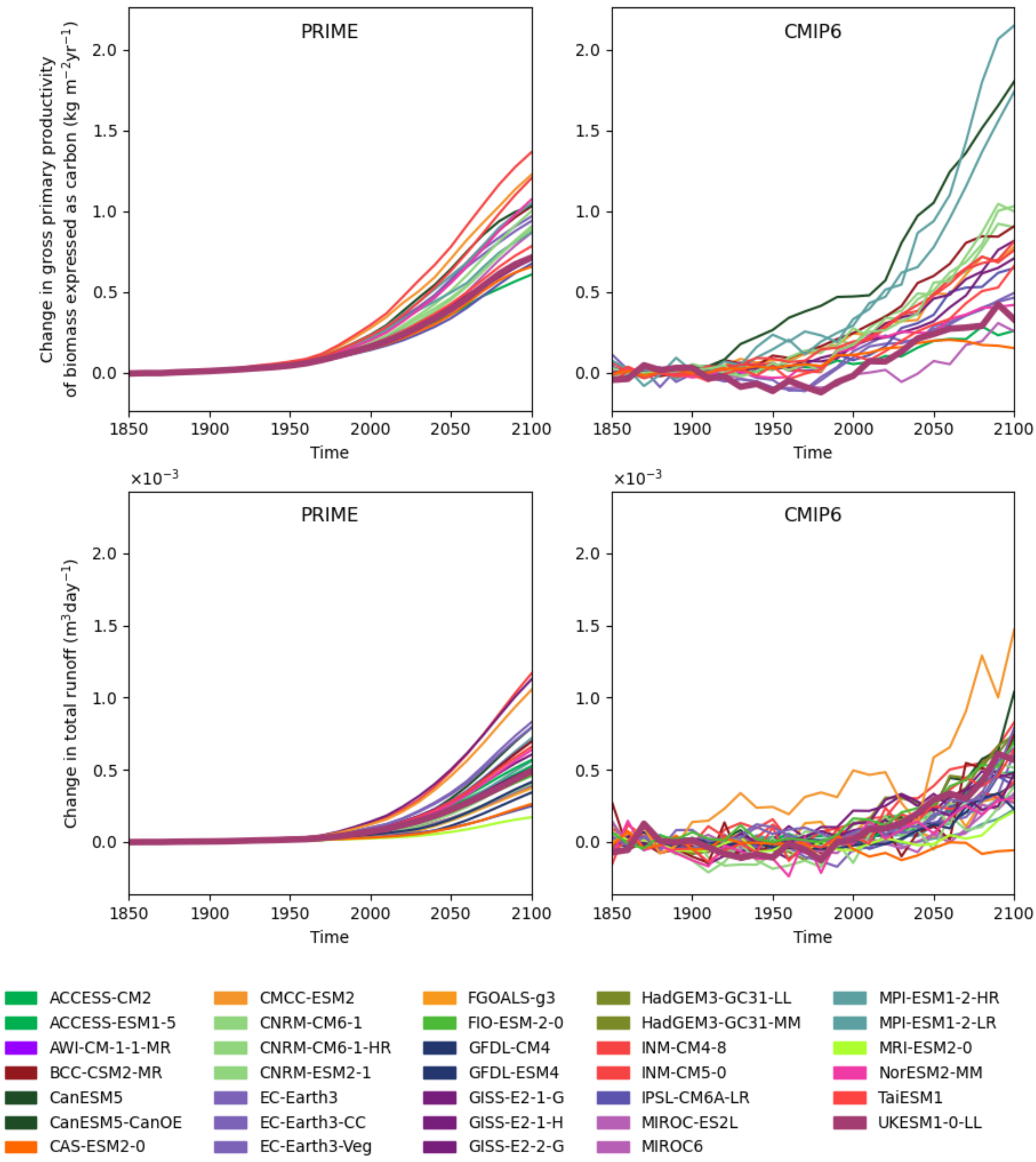

Figure S33. Timeseries of the change in gpp (top) and change in total runoff (bottom) for PRIME (left) and CMIP6 (right) for SSP5-8.5, the training scenario for the USA region for each CMIP6 model

Table S1. SSP5-8.5 driven CMIP6 model patterns, selected based on data availability.

	Model	Realisation
1.	ACCESS-CM2	r1i1p1f1
2.	ACCESS-ESM1-5	r3i1p1f1
3.	AWI-CM-1-1-MR	r1i1p1f1
4.	BCC-CSM2-MR	r1i1p1f1
5.	CAS-ESM2-0	r1i1p1f1
6.	CMCC-ESM2	r1i1p1f1
7.	CNRM-CM6-1	r1i1p1f2
8.	CNRM-CM6-1-HR	r1i1p1f2
9.	CNRM-ESM2-1	r1i1p1f2
10.	CanESM5	r1i1p1f1
11.	CanESM5-CanOE	r1i1p2f1
12.	EC-Earth3	r11i1p1f1
13.	EC-Earth3-CC	r1i1p1f1
14.	EC-Earth3-Veg	r1i1p1f1
15.	FGOALS-g3	r1i1p1f1
16.	FIO-ESM-2-0	r1i1p1f1
17.	GFDL-CM4	r1i1p1f1
18.	GFDL-ESM4	r1i1p1f1
19.	GISS-E2-1-G	r1i1p5f1
20.	GISS-E2-1-H	r3i1p1f2
21.	GISS-E2-2-G	r1i1p3f1
22.	HadGEM3-GC31-LL	r1i1p1f3
23.	HadGEM3-GC31-MM	r1i1p1f3
24.	INM-CM4-8	r1i1p1f1
25.	INM-CM5-0	r1i1p1f1
26.	IPSL-CM6A-LR	r1i1p1f1
27.	MIROC-ES2L	r1i1p1f2
28.	MIROC6	r1i1p1f1
29.	MPI-ESM1-2-HR	r1i1p1f1
30.	MPI-ESM1-2-LR	r1i1p1f1
31.	MRI-ESM2-0	r1i1p1f1
32.	NorESM2-MM	r1i1p1f1
33.	TaiESM1	r1i1p1f1
34.	UKESM1-0-LL	r1i1p1f2